RUSSIAN ACADEMY OF SCIENCES

SIBERIAN DIVISION

LAVRENTYEV INSTITUTE OF HYDRODYNAMICS

REPORT LIH -10-98

CURRENT INSTABILITY AND DISRUPTION OF SHAPED-CHARGE JETS

(final report)

G. A. Shvetsov, A. D. Matrosov

NOVOSIBIRSK

1998

This report is prepared according to the contract SPC-98-4019 between the Lavrentyev Institute of Hydrodynamics of the Russian Academy of Sciences and the European Office of Aerospace Research and Development (EOARD).

CONTENTS

CURRENT INSTABILITY AND DISRUPTION OF SHAPED-CHARGE JETS

G. A. Shvetsov, and A. D. Matrosov

Lavrentyev Institute of Hydrodynamics, Siberian Division,
Russian Academy of Sciences, Novosibirsk, 630090, Russia

• "It can be readily shown that upon a sinusoidal disturbance of a free jet, disturbance "waves" will grow without bound, i.e., the motion is unstable. The most interesting fact is that with allowance for arbitrary small viscosity, "waves" of large amplitude cannot occur - the real liquid thus ensures "limited stability." I believe that a detailed study, qualitative and quantitative, of all these "instabilities and stabilities" will be of much interest."

•• "The abrupt decrease in the penetrating effect upon an increase in the distance between a shaped charge and a target is primarily explained by the instability of the jet."

M.A.Lavrentyev, "Cumulative Charge and Principles of Its Work", Usp. Mat. Nauk, Vol. 12, No. 4, 41-56 (1957).

INTRODUCTION

The idea of electromagnetic action on a shaped-charge jet (SCJ) has a relatively long history. The first experiments familiar to the authors were performed under the guidance of M. A. Lavrentyev as early as 1957 [1]. In these experiments, small shaped charges (SC) of caliber 25 mm were used. A capacitor bank with a voltage of up to 50 kV was used as the electromagnetic energy source. The problem has not been studied in detail, but these experiments showed that a SCJ can be destroyed by passage of a high electric current through it, which leads to a decrease in the penetration depth.

At the end of the 1970s, comprehensive studies of the stability of SCJ with passage of an axial electric current through them were began at the Institute of Hydrodynamics [2÷4]. The experiments have shown that SCJ are unstable in the magnetic field of an axial current. The instability detected in the experiments was called "current instability of shaped-charged jets" [3]. Later other teams of scientists began to work in this line.

At present, a great number of works concerned with this physical phenomenon have been published. A review of the main publications of authors from Russia (Soviet Union) is given in this report.

1. GENERAL DIAGRAM AND FEATURES OF EXPERIMENTS ON THE INSTABILITY OF JETS IN THE MAGNETIC FIELD OF THE AXIAL CURRENT

A diagrams of most of the experiments described below are shown in Fig. 1a,b, where 1 is a SC, 2 is the source of electromagnetic energy, 3 are the electrodes, 4 are the inductive probes used to measure current and the current derivative of the discharge. Sites of X-ray photography are marked by 5. In the diagram in Fig. 1b, the lower electrode is simultaneously a target. Current begins to pass through the SCJ since closure of the electrodes by the jet.

Let us consider some features of experiments on heating of elements of SCJ and diffusion of a magnetic field in the jet. When a SCJ penetrates into a plate (upper electrode), the hole diameter exceeds several fold the SCJ diameter, and the electric contact between the jet and the electrode is an electric arc. In this case, the jet elements are heated not only by an internal source (Joule heating) but also by an external source (electric-arc heating). In diagram 1 (Fig. 1a), arc contacts occur at the upper and lower electrodes. In diagram 2 (Fig. 1b), one can assume, under certain conditions, the existence of a metallic "jet-electrode" contact at the bottom of the cavern formed (see Fig. 28b). In this case, a current (or main part of the current) passes through the jet and the internal surface of the cavern formed during penetration of SCJ. If this is the case, the time of electromagnetic action on the jet element in diagram 2 can be longer than in diagram 1.

Unlike a stationary "explosive" solid conductor, heating of each element of the jet begins at different moments when the element begins to experience a current flow. The conditions of diffusion of a magnetic field into SCJ elements are not identical at different times and depend on the current-pulse amplitude and shape and on the duration of exposure of an element to current.

The main property that determines the SCJ behavior in a magnetic field is the electrical conductivity of the jet material. Note that the initial SCJ temperature is on the order of 500÷900 °C and the temperature distribution over the radius and length of the jet remains unknown. The quickness of magnetic-field variation in time (the speed of penetration of the magnetic field into the SCJ material) is also of significance. According to the characteristic thickness of the skin-layer, electromagnetic actions on SCJ can be classified as high-skin actions (the skin-layer thickness is far less than the SCJ radius) and low-frequency actions (a magnetic field penetrates into the entire depth of the SCJ material).

The features of magnetic-field diffusion into a SCJ determine the degree of uniformity in the temperature distribution over the SCJ radius. Note that the problem considered include "forward" diffusion of a magnetic field into a conductor (during passage of a current through SCJ elements)

and "reverse" diffusion of the magnetic field from the conductor when the SCJ elements leave the interelectrode gap. In the first case, the conductor is compressed by electromagnetic forces, and in the second case, it is stretched in the radial and axial directions.

The indicated features of heating of SCJ and magnetic-field diffusion are important integral parts in understanding of the physical pattern of the processes occurring in a SCJ with passage of an electric current through it.

2. RESULTS OF EXPERIMENTAL STUDIES OF THE CURRENT INSTABILITY OF SHAPED-CHARGE JETS

Experiments with 30 to 100-mm diameter charges with a conical copper liner are described in [2÷7]. A capacitor bank with a charge voltage of up to 5 kV and a capacitance of up to 20 mF was used as the energy source. A current starts to flow in a SCJ after closure of the electrodes by the jet. The current and discharge current derivative (100÷500 kA, $3 \cdot 10^9 \div 10^{11}$ A/s), the electric-pulse duration, the time of action on the various parts of the jet, and other parameters were varied in the tests. Flash radiography of the SCJ in free flight and in a target (aluminum) was carried out. Flash radiography in the experiments with and without a current was performed with an accuracy of not worse than 0.5 μs for the same time. The effect of an electric current on a SCJ was additionally determined from jet penetration into the target.

Figure 2a, b shows radiographs of two tests with a SC of diameter 50 mm: a) experiment without a current, b) experiment with a current (450 kA). A diagram of the experiments is shown in Fig. 1b. A target made of aluminum alloy was one of the electrodes. It should be noted that at the flash moment the cavern depths were approximately equal. In the experiment with a current, the jet broke into separate fragments.

Figure 3a-e gives pairs of radiographs of a jet from a 50-mm SC with and without a current (the left and right radiographs, respectively), taken at different times. It can be seen in the radiographs beginning from Fig. 3b that, in experiments with a current, SCJ have discontinuities in front of the lower electrode with noticeable thickening along the jet diameter above the discontinuities. Figure 3f scales up the portion of the SCJ ahead of the lower electrode from Fig. 3c. The appearance and development of necks are also evident in the radiographs. After passing the lower electrode, the jet breaks into separate fragments with dimensions in the axial direction equal to approximately 1÷3 jet diameters. The fragments expand in the radial direction and reach 5÷10 jet diameters in the same cross sections as in experiments without a current. Qualitatively, the failure patterns of the SCJ from 30-, 50-, and 100-mm charges are the same. Figure 4a-d shows radiographs of jets from 100-mm SC: a) and c) experiments without a current; b) and d) experiments with a current.

An analysis of radiographs of the same jet cross sections taken at the same time shows that the number of fragments in experiments with a current is roughly the same as the number of necks in the jet without a current.

The above catastrophic behavior of SCJ with passage of an electric current through them leads to a severalfold decrease in the cavern depth in the target. This process can be controlled by varying the current amplitude, the current derivative, and the electric-pulse duration. Figures 5 and 6 show the penetration of a jet from a 50-mm diameter SC into steel (Fig. 5) and aluminum (Fig. 6) targets versus the current amplitude for the same discharge-current derivative and electric-pulse duration. Comparison of the experimental data in Figs. 5 and 6 shows that the final depths of caverns in experiments with steel and aluminum targets differ little in absolute measurement (by about 20-30 mm), whereas in control experiments (without a current), the difference between them was about 170 mm). Figure 7 gives cavern depths in a steel target obtained in experiments with a 30-mm diameter charge.

Figure 8 presents results of two experiments with an aluminum target using a laboratory SC of diameter 100 mm. The depth of a cavern in a control experiment was h_0 = 680 mm. In an experiment with a current (430 kA), it was h = 300 mm.

Results of experimental studies performed by the team of A. I. Pavlovskii are reported in [8, 9]. The experiments were performed in two modes: a moderate current mode and a high current mode. The goal of experiments in the high current mode was to optimize a current generator for some depths of SCJ penetration into the target, and the experiments with high currents were aimed at minimization of the cavern depth and complete disruption of SCJ.

A diagram of experiments in the moderate current mode is shown in Fig. 9. In the experiments, use was made of an additional inductance (~ 5÷10 μH), on which a capacitor bank begins to discharge 20÷30 μsec before the SCJ closes the gap between the electrodes. After closure, the current through this inductance can be ignored. The electric contact between the upper electrode and the SCJ is an arc discharge.

The derivative dI/dt of the discharge current was measured by an inductive probe, and the voltage U across the electrodes, by an ohmic divider. Typical oscilloscope traces are shown in Fig. 10. The current $I(t)$ in the SCJ and the total resistance $R(t)$ of the subcircuit between the electrodes were calculated from these oscilloscope traces:

$$I(t) = \int_0^t (dI/dt)\,dt, \qquad R(t) = \{U - (U_0/dI_0/dt)dI/dt\}/I(t).$$

Here dI_0/dt is the value of the current derivative after closure of the electrodes by the SCJ and U_0 is the voltage across the electrodes at this moment.

The maximum depth of the cavern pierced in the target (steel 3) by the SCJ from charges with a cone diameter of 45 mm is 195÷210 mm. The experimental time dependences of the growth in

the cavern depth and of the SCJ tip velocity at this depth are given in Fig. 11. The maximum cavern depth for the second charge (for a 115 mm diameter charge) is ~ 600 mm.

The results of some experiments with the SCJ from both charges are summarized in Table 1, which gives the liner diameter D, the capacitance of the capacitor bank C, the charge voltage U_C, the maximum current I_{max}; T is the the time from the closure of the electrodes by the SCJ to the maximum current, and h is the cavern depth in the target. The curves of $I(t)$ and $R(t)$ for some of these experiments are given in Fig. 12. Figure 13 shows sections of the caverns obtained in some experiments.

Radiography was performed as shown in the diagram in Fig. 1a. In this case, the electric circuit in the lower electrode is closed by a arc discharge, and the current acts only on the interelectrode gap. After this, the SCJ passes into the air and the results of this action can be observed. The authors note that, in this variant of disruption, the conditions of SCJ disruption change because of a reduction in the time of current action on the SCJ elements. Nevertheless, the disruption process can be visualized qualitatively by the picture obtained.

Table 1

Experiment number	D, mm	C, μF	U_C, kV	I_{max}, kA	T, μs	h, mm
1	45	6000	15	710	22	50
2	45	6000	10	430	30	90
3	45	1500	15	500	38	110
4	100	6000	23	1700	38	205
5	100	6000	21	1200	43	250
6	100	900	30	850	33	300

Some radiographs are given in Fig. 14. The current curves in these experiments approximately coincide with curve 2 (Fig. 12), except for experiments (Fig. 14a and b), in which the current was diminished; the flash times are shown on curve 2. Figure 14b shows well-developed necks in the jet, while in Fig. 14c, necks are evident only at the SCJ tip. When the jet passes through the interelectrode gap, the necks in the other regions of the jet are destroyed to form strata. For the SCJ elements that leave the interelectrode gap, disruption of the necks is of an explosive character and strata are formed. This is clearly seen in the next photographs (Fig. 14d and e). In this case, SCJ disruption already proceeds in the gap between the electrodes.

In [8], the process of disruption of a SCJ is conditionally divided into three phases.

"The first phase involves disruption of the SCJ tip. After closure of the circuit, the current in the SCJ begins to grow from zero, the elements of the jet tip are consumed without receiving a current integral of action necessary for disruption of necks. After attainment of a critical value of the integral of action, formation and disruption of necks begin, and the fragments formed no longer increase the depth of the cavern. If this continues to the end of the process, the depth of the cavern obtained in the first phase will be the final. It will decrease only with increase in the speed of current build-up. If this occurs as a result of rise in voltage of the capacitor bank, the dependence of the cavern depth on the energy of the battery will not be linear in this case."

"In the main (second) phase, the disruption zone is usually displaced from the bottom of the cavern formed upon disruption of the SCJ tip to the electrodes and in the interelectrode gap because with current build-up, the required action will be attained earlier. Even the current decay that begins is initially compensated for by a decrease in the velocity of the SCJ elements."

"The character of disruption in the final (third) phase will be different," as noted in [8], "if the current-pulse duration is markedly shorter than the time required for passage of the entire SCJ length between the electrodes. With a decrease in current, the zone of disruption of a SCJ begins to move from the electrode along the cavern. If the current decays rather rapidly, the jet reaches the bottom of the cavern and participate in penetration through the target. In this case, a typical shape of cavern consisting of a narrow projection and a wide cavity forms, as shown in Fig. 13c."

It is also noted in [8] that, "because of the asymmetric current lead due to the action of ponderomotivie forces, the SCJ elements acquire a lateral pulse, which, at a sufficiently high current, can have an effect on formation of the cavern." However, this effect was not observed in the experiments described in [8].

A diagram of experiments in the high-current mode is given in Fig. 15 [9]. It is analogous to the previous diagram (see Fig. 9). The part of the target of thickness S was varied in the experiments. Experimental results are summarizes in Table 2, which gives the capacitance of the capacitor bank C , the charge voltage U_C, the maximum current I_{max}, the time during which the current increases from zero to maximum T, the thickness S and average density of the target ρ_{av} in the region S, and the penetration depth h.

Experiments 1-10 were performed with a charge with a 45-mm diameter liner, F = 55 mm, H = 30 mm. In experiments 11 and 12, a charge with a 100-mm diameter liner was used; F = 115 mm, H = 45 mm. Some experimentally obtained curves of the current in the SCJ $I(t)$ and resistance curves of $R(t)$ for the subcircuit between electrodes 3 and 4 are given in Fig. 16.

In experiment 1, the space S is occupied by an air gap, and electrode 4 is placed directly on the collector target 7, so that the spacing between the electrodes in this experiment is increased to 110 mm. Without a current in this case, the cavern depth was 150 mm. It can be seen from Fig. 16 that the resistance suffers large jumps, which disturb the shape of the current pulse and decrease its amplitude. During disruption of the SCJ, the contacts between individual fragments are maintained by arc discharges. The resulting region of intense disruption gives an increases in the resistance. This region is displaced toward to the buttom of target by motion of the SCJ, and the resistance decreases again. Then, a new region of disruption can form, etc. As a result the cavern depth increased from 50 to 65 mm in the experiment.

Experiments 2-4 were performed to obtain a possibility of contact of the SCJ with the lateral surface of the cavern under strong disruption of the jet. In this case, the space S was filled with duralumin, powder cooper, and porous aluminum produced by methods of powder metallurgy. Table 2 gives depths of thus produced caverns in a steel target. In experiment 4, the current curve is similar in shape to the curve in experiment 1. The electrical resistance in this experiment is even higher than in experiment 1. This is apparently explained by the larger diameter of the cavern in porous aluminum and its low conductivity.

Table 2

Experiment number	C, μF	U_C, kV	S, mm	ρ_{av}, g/cm^3	I_{max}, MA	T, μs	h, mm
1	900	20	80	2,7	0,36	38	65
2	900	20	80	1,4	0,51	30	15
3	900	20	80	1,2	0,43	30	23
4	900	20	80	0,9	0,38	38	37
5	900	25	150	1,8	0,65	32	50
6	900	20	150	1,8	0,33	32	20
7	900	25	150	1,8	0,52	32	3-5
8	900	25	150	0,2	0,56	32	3-5
9	900	20	150	0,2	0,47	32	10
10	900	25	150	1,8	0,47	35	3-5
11	6000	21	200	0,3	1,32	50	110
12	6000	21	200	2,6	1,6	68	3-40

In experiments 5-12, the space S was filled with a set of metallic plates located parallel to the jet, with an air gap between them. Radiography of the jet under the action of current was performed from the lateral edge of the plates (see below). In experiment 5, copper plates 1 mm thick spaced at 10 mm were used. The flash moments are shown on curve 5 (Fig. 16).

Figure 17 gives X-ray photographs of SCJ disruption taken in these experiments. Figure 17a shows the initial stages of disruption. From the radiograph in Fig. 17d, taken 25 μsec after the beginning of discharge of the capacitor bank on the SCJ in experiment 6, it can be seen that only a small portion of the jet remains undestroyed (shown by the arrow), and the main part of the jet is disrupted near the electrodes. The jump in the resistance on curve 6 (Fig. 16) approximately coincides in time with separation of this undestroyed portion of the jet, as can be seen in the photograph. When a higher current was used (experiment 7), the photographs do not show undestroyed jet regions, and the zone of jet disruption occupied not more than 30 mm of the plate length. Obviously, a reduction in the dimension of S to ~ 40 mm in this experiment would not influence the result of an experiment in which complete jet destruction occurred. A cavern was practically absent, and only several holes 3÷5 mm deep remained on the steel surface. Thus, the possibility of complete SCJ disruption has been demonstrated experimentally [9].

The slope of a SCJ to the plane of electrodes increases instability in the initial stages of development of a stable current circuit. It is noted in [9] that further studies of the effect of various factors on the current disruption of a SCJ in its various stages are required.

In [8, 9], the authors used a SC with a low velocity of the SCJ tip (about 8 km/sec). Recently, the authors performed experiments on jet disruption in a high-current mode at a high velocity of the SCJ tip (to 12 km/sec). Results of the experiments will be described in [10].

Experiments on SCJ disruption by a current using an explosive magnetocumulative generator (MCG) as a power source are described in [11,12].

Advantages of MCG are small dimensions and the possibility of obtaining large energies and currents with such dimensions. This allows MCG with SC of large and small diameters to be used.

There are, however, two significant differences of an MCG from a capacitor bank. Whereas, in a capacitor bank, electric energy has already been accumulated and begins to release to the SCJ after closure of the electrodes by the jet, with use of MCG, some time is required to convert explosive energy to electric energy. Therefore a system of synchronization of the operation of a SC and MCG is required.

The primary winding inductance of the transformer is 18 nH, and the final total inductance of the primary circuit is 18.4 nH. The number of turns in the secondary winding of the transformer is decreased to 7.5. The experimental current curve for this generator under a purely inductive load of 0.15 μH is given in Fig. 19 (curve 1). Figure 20 shows the corresponding current curve in the MCG circuit for this case (curve 1).

The inductance was the same (0.15 μH) as the inductance of an analogous device in experiments with a capacitor bank. It can be seen from these experiments that the load resistance introduced by the jet and its contacts with the plates varies from 5 to 8 mOhm in experiments with 55-mm charges and to 10 mOhm in experiments with 100-mm charges. This value is high enough to have an effect on the operation of the generator but is not sufficiently high that the approximation of effective inductance cannot be applied to estimation of MCG operation.

The time of explosion of SC was chosen so that SCJ closes the contact plates at a given time t^*. In the experiments, 55-mm SC (the penetration depth h_0 in steel is 190÷210 mm) and 100-mm SC (h_0 = 460 mm) were used.

Results of the experiments are given in Table 3. The current curves for SCJ obtained in experiments No. 1 and No. 2 are given in Fig. 19 (curves 2 and 3 respectively), and those obtained in experiments No. 3 and No. 5 are given in Fig. 21 (curves 2 and 1 respectively).

Table 3

Experiment number	D, mm	t^*, μs	I_{max}, kA	h, cm	h_0/h
1	55	36	600	5,5	3,5
2	55	8	200	5,5	3,5
3	100	13	290	31	1,5
4	100	16	350	25	1,9
5	100	26	430	27	1,7

Figure 22 shows photographs of sections of a cavern in a steel target in experiments with 100-mm SC: a) experiment without a current, b),c), and d) experiments No. 3, No. 4, and No. 5, respectively (Table 3).

A section of a cavern produced in a steel target in experiment 1 is presented in Fig. 23. In experiment 1, the current front is plane (whereas in experiment 2, a current of 200 kA is attained for 8 μsec, in experiment 1, it is attained for 36 μsec). Therefore, the shape of the cavern is determined by the initial part of the pulse. In experiment 2, the narrow curvy channel is formed at

3. A QUALITATIVE PHYSICAL MODEL FOR DISRUPTION OF A SHAPED-CHARGE JET BY AN ELECTRIC CURRENT AND DECREASE IN THE CAVERN DEPTH

Before proceeding to description of the qualitative physical model, some remarks should be made.

1). It is known [19,20] that the jets formed in detonation of SC are unstable and show tendency to neck formation (local constriction) and to disruption into individual fragments.

2). Interaction of the current flowing through a conductor with the internal magnetic field produces radial and axial forces, whose action leads to radial compression of the conductor. Simultaneously, in the presence of necking, the conductor is compressed and stretched in the axial direction (in Fig. 26 the forces F_1 and F_2, respectively). It should be noted that the magnetic pressure

$$p = B^2 / 2\mu_0 = \mu_0 I^2 / 8\pi^2 r^2$$

(r is the jet radius) can be much higher in the necking zone than in the convexity zones, and, therefore, the magnetic pressure will enhance the initial necking instability of the jet.

The magnitude of the magnetic field for which magnetic pressure creates mechanical stresses in a metal that correspond to the yield strength Y is defined as the yield field:

$$B_Y = (2\mu_0 Y)^{0.5}$$

The corresponding linear current density is

$$(I/r)_Y = 2\pi (2Y/\mu_0)^{0.5}.$$

For some materials, the magnitudes of the "yield field" B_Y and the linear current densities $(I/r)_Y$ are presented in Table 4. The physical meaning of B_Y is obvious. For $B < B_Y$, elastic deformations occur and for $B > B_Y$ plastic deformations take place. In the latter case, one might expect that accelerated growth of necking and breakup of metallic SCJ occur under relatively low currents. It should be noted that the values of B_Y and $(I/r_0)_Y$ presented in Table 4 should be regarded only as estimates, since they were obtained for static values of yield strength at 20 °C [21]. To estimate the yield field in the case of SCJ, one should use the values of dynamic yield strength of the material, which are somewhat higher than the static values, and take into account the dependence of the yield strength on the jet temperature. Fig. 27 gives the curves of $\sigma(\varepsilon)$

obtained by the authors of this report for copper at different initial temperatures of specimens (20÷1000 °C) and an average strain rate of ~ $3 \cdot 10^{-1}$ sec^{-1}. It follows from Fig. 27 that, at temperatures of 600÷1000 °C, the yield strength of copper decreases by a factor of 9÷19, and, accordingly, one might expect a severalfold decrease in the values of B_Y and $(I/r_0)_Y$.

Note also that the SCJ temperature is about 500÷900 °C [19,20]. One might expect that in experiments with passage of a current through a SCJ, the temperature of the jet (of its elements) would be higher.

If the above remarks and estimates are valid, for currents of $(3 \div 5) \cdot 10^5$ A and r_0 = 1 mm (r_0 is the SCJ mean radius), the yield strength will be only several percent of the magnetic pressure. Under these conditions, a SCJ can be treated as an incompressible, conducting, perfectly plastic fluid.

Table 4

Material	$Y \cdot 10^9$, Pa	B_Y, T	$(I/r_0)_Y$, kA/mm
Aluminum	0,022	7,4	37,3
Silver (anneal.)	0,02-0,03	7,9	39,7
Copper (anneal.)	0,07	13,3	66,5
Copper	0,2	22,6	112,3
Nickel (anneal.)	0,08	14,2	71,1
Titanium (apart. pure)	0,1	15,8	79,4
Iron	0,17	20,7	103,6
Steel 3	0,22	23,8	119,2
Tantalum (anneal.)	0,4	31,8	158,9
Molybdenum (anneal.)	0,57	37,7	189,7
Tungsten (deform.)	0,76	43,9	219,0

3). One can assume that the process of development of necking will continue until the current density in the necks reaches a value for which electric blasting of the necking occurs, which, in turn, imparts an additional pulse to the upstream and downstream elements of the jet (Fig. 26). When a SCJ leaves the interelectrode gap, jet compression by magnetic pressure ceases. In this case, as follows from the radiographs (Figs. 3 and 4) radial expansion of the jet can occur.

The experiments performed and the above-mentioned physical considerations allowed the authors to propose a qualitative physical model for the development of current instability in SCJ and penetration depth reduction [6].

After closure of electrodes by a jet, a current begins to flow through the jet (Fig. 28a). If the current amplitude and duration of the electrical effect do not exceed some critical values, current instability does not develop in the jet (Fig. 3a) and the penetration depth does not differ from the control value (Figs. 2a and b, 5a and b, and 7a and b). Assume that at time t_1 (Fig. 28b) the current value I^* is such that current instability develops when the current flows through the jet elements located above the upper electrode at this time. In this case, the final penetration depth will be defined as the SCJ length from the upper electrode to the bottom of the cavern (Fig. 28b). Clearly, the shorter the time required to reach the critical current value (the larger the current derivative), the shorter the length of the jet that passes through the electrodes without disturbances, and the smaller the penetration depth. A typical cavern shape in this case is shown in Figs. 5e and 7e. If at some time after the moment t_1 the current in the circuit becomes smaller than its critical value, current instability develops solely in the mid-sections of the jet. The tail sections of the jet can additionally contribute to the penetration depth. The cavern in this case has the typical shape shown in Figs. 5c and 7c.

When an SCJ element is present in the region of passage of an axial current, compressing electromagnetic forces prevent expansion in the radial direction. However, when the SCJ elements leave the interelectrode subcircuit, the preventing effect of the electromagnetic forces disappears, and the compressed jet material acquire a velocity directed from the axis. In the process, volume compression and loss of continuity of the jet material occur. Similar conclusions were drawn in [18, 22].

4. NUMERICAL SIMULATION OF THE BEHAVIOR OF A SHAPED-CHARGE JET WITH PASSAGE OF A CURRENT THROUGH IT

A physicomathematical model for the stretching of an SCJ element under conditions of passage of a pulsed electric current is proposed in [22]. The model is realized within the framework of a quasi-two-dimensional axisymmetric problem of deformation of a compressible, elastoplastic, conducting, high-gradient bar stretched under inertial load, i.e., a given initial gradient of the axial velocity. The main features of the pulsed electromagnetic action on the SCJ elements are studied on the basis of a numerical solution of the problem using finite-difference methods.

The model is based on the assumption that during the deformation process the SCJ elements retain their cylindrical shape, and the gradients of the axial velocity V_0 between the fixed plane cross sections that bound the elements remained unchanged in time and are determined by the initial gradient of the axial velocity. In this case, the deformation of any isolated element of the jet can be considered in reference system attached to one of the plane cross sections that bound the element, and the time of formation of the element can be taken as zero time reference. In addition, it is assumed that the axial velocity distribution over the time-dependent element length is linear. As a result, identical deformation conditions are reproduced in each of the plane cross sections of the isolated element. It is, therefore, possible to study the behavior of the SCJ for two cases: 1) during purely mechanical stretching of the jet (up to the beginning of current action on the element) and 2) under electromagnetic action within the framework of solution of the essentially one-dimensional nonstationary problem.

The physicomechanical properties of the high-gradient bar material were described by the Mie-Gruneisen equation of state and the Prandtl-Reis equations of plastic flow for an ideal elastoplastic medium. The Mises criterion was used as the condition of plasticity. The mechanical behavior of an incompressible, rigidly plastic medium was described by the Saint-Vienant-Levi-Mises equations. The temperature curve of the electric resistivity of the material was linear.

The deformation of an elongating jet was analyzed prior to the beginning of electromagnetic action, during electromagnetic action, and after completion of the action. Calculations showed

that the changes in the stress and radial velocity of the outer surface of the SCJ elements in purely mechanical stretching have distinctive features of an ordered oscillation process.

The authors believe that the existence of an oscillation process during elongation of SCJ, as shown by the calculation, does not result from calculation effects but reflects the actual processes that occur in the jet. The authors attribute the existence of oscillation to the compressibility and inertial properties of the SCJ material. With passage of a current through the jet, the oscillation process continues, but against the background of overall compression by the magnetic field.

When a SCJ element leaves the interelectrode gap, the preventing action of the electromagnetic forces disappears and the compressed jet material acquires a velocity directed from the axis.

The "forward" diffusion of a magnetic field into a high-gradient bar after generation of a magnetic field on the bar surface and the reverse diffusion occurring after disappearance of the field from the surface when the SCJ elements leave the interelectrode gap were also analyzed. The radial ponderomotive forces arising during the diffusion process were compared with typical values of radial accelerations of the bar particles during bar deformation under an axial-velocity gradient in the absence of a magnetic field. Temperature calculation for the middle SCJ element for a jet of radius r = 1.2 mm with passage of a current of 350÷360 kA for 6-μsec residence of the element in the interelectrode gap showed that the temperature distribution over the jet radius is essentially nonuniform. The near-axis region of the jet is in the solid state, and the peripheral region is in the molten state. Calculations showed that the SCJ element that leaves the region of action is almost uniformly heated (T = 2200÷2450 °C) and is in the molten state.

Clearly, material that exists in such a state cannot resist shape changes and, from the viewpoint of mechanical behavior, should behave as a liquid, and its stressed state should be completely characterized by one scalar quantity, namely, the pressure p. The authors believe that like a liquid, such a material cannot withstand conditions of overall extension, and the occurrence of negative (tensile stresses) entails violation of material continuity, i.e., failure and loss of ability to withstand deformation (volume destruction model).

Results of physicomathematical modeling of the behavior of SCJ with passage of a powerful current pulse were generalized in [23,24]. These investigations are a continuation of the analytical and numerical modeling began by Babkin et al. [25] using the assumption of volume destruction of SCJ under the action of a current pulse.

These papers give a comparison of the analytical and numerical estimates of the radial expansion velocity of the SCJ material (Fig. 29) as a function of the discharge current. In

addition, results of numerical modeling and experiments [8] are compared and curves of $h(t)$, $V_z(t)$ and $I(t)$ [8] together with curves obtained numerically (Fig. 30, Fig.12b) are presented.

Table 5 compares the calculation results with the experimental results of [8] for the penetration depth L of the main target subjected to various SC and for current pulses with various I_{max} and for various times t_{max} required to attain a current maximum. As can be seen from Table 5, except for experiments 3 and 4, the calculation results are in fair agreement with the experimental data (d_0 is the conical liner diameter and Δ is the difference between the calculation and experimental results).

Table 5

Experiment number	d_0, mm	I_{max}, kA	t_{max}, μs	L_{exp}, mm	L_{cal}, mm	Δ, %
1	45	710	22	50	47	7
2	45	430	30	90	84	6
3	45	500	38	110	68	38
4	100	1700	38	205	147	29
5	100	1200	43	250	213	14
6	100	850	33	300	320	7

Figure 25 shows a time-space diagram of the interaction of the SC with a target, constructed for the case of electrodynamic action on the SCJ with parameters as in experiment 1 from Table 5. From analysis of this diagram, Babkin et al. [24] infer that the elements of the middle and tail parts of the SCJ, subjected to the most intense action of an electric current, do not contribute to the penetration depth. This can be seen in Fig. 31, which shows curves of increase in the penetration depth L in the form of distributions in the relative initial length $\bar{z}_0$ of SCJ in sequential operation of jet elements from tip elements ($\bar{z}_0 = 1$) to tail elements ($\bar{z}_0 = 0$). The curve numbers correspond to the experiment numbers in Table 5, and the curve with subscript "0" corresponds to the case where an electrode system plays a purely passive role ($I_{max} = 0$).

Similar conclusions can be drawn from analysis of distributions of the radial velocity V_R of scattering of the jet material after volume destruction versus current (Fig. 32).

Thus, Babkin, et al. [22, 23] believe that one of the available hypothesis on SCJ destruction by a current pulse, based on the concept of volume destruction received additional substantiation. The authors of [23] believe that the hypothesis on the development of MHD instability is also justified.

In [23,24], physicomechanical modeling was performed using two physicomechanical models (volume destruction and MHD instability) within the framework of a numerical solution of quasi-two-dimensional nonstationary problems of dynamic deformation of a high-gradient, conducting, thermally weakening bar with a given law of time variation in the total current passing through the bar.

The mechanism of volume destruction was considered within the framework of a cylindrical compressible elastoplastic bar under the assumption of the absence of necking on the SCJ elements (model 1) [18]. This model was described above.

Numerical values of the radial scattering velocity of the jet material after emergence from the interelectrode gap are shown in the curves in Fig. 33, which were constructed for uniformly deformed elements of the middle part of the SCJ from 50-mm and 100-mm SC subjected to electrodynamic action at distances of 2 or 3 diameters from the SC. As can be seen from the curves, sufficiently intense electrodynamic action can lead to radial scattering of the SCJ material at a considerable velocity and to weakening of the SCJ material. Also, without changing the kinetic energy of the axial (directed toward the target) motion of the jet, this action can change the jet "structure", smear it, and decrease the energy concentration at the moment of energy release at the target. At the same time, the ability of the low-density SCJ elements to penetrate through a strong target decreases with increase in the degree of weakening of the material, according to the concept of the critical velocity of penetration.

MHD instability was studied using a physicomathematical model, in which SCJ elements are treated as regions of an incompressible, rigidly plastic, thermally weakening, varying-section bar ignoring the possible volume destruction of the material (model 2). This model is based on the assumptions of plane sections. It is assumed that the current density is distributed uniformly over the cross sections, and the action of the current was taken into account by specifying magnetic pressure on the surface of an SCJ element.

The development of MHD instability was considered for elements of the middle part of a SCJ from 50-mm and 100-mm charges from the beginning of natural necking in the SCJ. In this case, at the initial moment, a small harmonic disturbance was assigned on the high-gradient bar that models the SCJ element.

The calculations showed that electrodynamic action not only accelerates the development of plastic instability on the SCJ, leading to its rapid fragmentation, but, at sufficient intensity, can cause the "disk formation" phenomenon. This phenomenon involves intense axial compression of material in jet regions with initially small bulges, accompanied by an increase in the radius of

these regions. Figure 34 shows the evolution of the shape of the elements of a SCJ from a 50-mm SC under free deformation (Fig. 34a) and under the action of current $I = 400$ kA for $\Delta t = 5$ μsec (Fig. 34b). Typically, under this short action of current, the "disk formation" process manifests itself only slightly under electrodynamic load and, because of the inertial properties of the material, it is realized only after the SCJ elements leave the region of action. In the development of MHD instability, as shown by calculations, a strong scale effect is pronounced.

5. INFLUENCE OF A LONGITUDINAL MAGNETIC FIELD ON AN ELONGATING SHAPED-CHARGE JET

Fedorov et al. [25÷27] analyzed the possibility of controlling shaped-charge explosion by electromagnetic action on the SCJ in free flight by means of a longitudinal, axisymmetric, spatially uniform magnetic field that slowly varies in time. This action was aimed at producing controlling forces in a deformed SCJ. These forces can influence the development of plastic instability in the jet, "decelerate" fragmentation of the jet, and thus increase the effective length, and, hence, the penetrating effect of the jet.

In these papers, a physicomechanical model was formulated to determine the external magnetic field at which ponderomotive forces that arise can compete with internal forces of mechanical origin and produce a stabilizing effect on the elongation of the SCJ in free flight. This model describes the behavior of a high-gradient, elastoplastic, conducting bar in a longitudinal magnetic field within the framework of the one-dimensional problem of the mechanics and electrodynamics of continuum.

The model in [26] is largely similar to the model [22] described in the first portion of section 4 of the present work. Here we shall not dwell on this model.

The results of the numerical calculations performed suggest that the magnetic field acting on a SCJ by the indicated scheme should have a magnitude of 1÷10 T. In this case, the corresponding ratio of the electromagnetic forces and the internal forces of mechanical origin is 0.1÷10. An increase in the inductance of the magnetic field in excess of the indicated range is not reasonable since the SCJ can break up at the moment it leaves the magnetic field region because of the occurrence of additional tensile stresses in the jet material at this time.

The variant of electromagnetic action considered by the authors was realized experimentally under laboratory conditions. A diagram of the experiment is given in Fig. 35. For the chosen solenoid diameter, the penetration depth averaged over 4-5 experiments in the absence of a magnetic field was $\bar{L} = L/d = 4.7$ with the best result of $\bar{L} = 4.9$ (L is the penetration depth and d is the SC diameter).

Table 6 gives results of experiments with electromagnetic action of various intensity. Except for electromagnetic actions, the other experimental; conditions were the same as in the series of experiments performed in the absence of a current.

As can be seen from Table 6, the results exhibit no regularity. However, in almost all the experiments, the penetration depth exceeds not only the average but also the maximum value obtained under comparable conditions without electromagnetic action. This excess is small. It is larger by 10% than the average value in only one experiment with a current. Nevertheless, some positive effect of a low-frequency electromagnetic field on a SCJ is observed. It is probable, as the authors of [25÷27] conclude, that more rationally organized electromagnetic action could lead to a more pronounced positive effect.

Table 6

Experiment number	t_m, μs	B_m, T	$\bar{L}$
1	120	2,6	5,5
2	140	3,3	4,6
3	200	5,4	5,3
4	140	6,3	5,1
5	140	10,5	5,0
6	140	10,5	5,2

Demidkov [28,29] proposed a method of contactless action by an external magnetic field on a SCJ that decreases the penetration depth.

It is proposed to expose a SCJ to a magnetic field at the stage at which the SCJ is a flow of individual elements. A diagram of the experiment is shown in Fig. 35. For the initial energy of a capacitor bank of 1.25 kJ, the penetration depths of SCJ from 50-mm charges were 35; 55; 55; 55; 75; 60 mm. At the same time, when the setup operated without a magnetic field, the penetration depths were 100; 175; 160; 130; and 96 mm. It follows from these data that the decrease in the penetration depth is detected despite the significant spread of the experimental data. In the authors' opinion, the decrease in the penetration depth is caused mainly by the magnetic-field gradient, which leads to turning of the SCJ elements.

6. POSSIBLE MECHANISMS OF DISRUPTION OF A SHAPED-CHARGE JET BY A CURRENT PULSE

In the above-mentioned papers three main hypotheses are proposed to explain the destruction of a SCJ with passage of a strong current pulse through the jet.

According to the first hypothesis in [18], a decrease in the penetrating ability of a jet through which a current is passed is explained mainly by thermal effects that weaken the jet material and change the conditions of penetration into the target. Yanevich et al. [18] indicate that two physically different situations are possible: 1) when $l_i < H$ (see Fig. 24), closure of the circuit leads to fragmentation of a SCJ element occurs under the action of thermal stresses; 2) When $l_i > H$, closure of the circuit causes spark discharges between the SCJ elements, and between the SCJ and the electrodes. In a time shorter than the time required to pass the gap between the electrodes, the spark discharge becomes an arc discharge, and this is responsible for electric-arc melting of the SCJ elements (the arc temperature reaches 5000 °C and higher). The authors mention the contribution of Joule heating to the melting of the SCJ elements but believe that it is less significant. The paper cited also emphasizes that the analogy between the disruption processes in the SCJ and liquid jets through which a current is passed is incorrect. In [18], doubt is cast upon the assumption that SCJ destruction is caused by the MHD instability of the jet.

The second hypothesis associates SCJ disruption and decrease in the depth of jet penetration with volume destruction of the material of a jet which leaves the interelectrode gap because of the joint thermal an mechanical action of the current. This action weakens the material, and leads to loss of ability to resist overall tension conditions that occur in the SCJ at a certain stage and to radial scattering of the material followed by a decrease in material density and penetration ability [18,23]. This volume destruction mechanism is reported in detail in section 4 and we shall not dwell on it here.

According to the third hypothesis, SCJ disruption occurs as a result of development of necking MHD instability in the jet [2÷9]. The hypothesis is based on experimental data and on X-ray patterns of a SCJ through which a current is passed. The X-ray patterns show the

occurrence of necks in the interelectrode gap. The number of necks in the jet without a current and the number of fragments of the SCJ through which a current is passed coincide with sufficient accuracy. This experimental fact leads to the conclusion that the action of an electric current results in an accelerated increase in the initial necking instability of jets. A more detailed description of the X-ray patterns was given in section 2.

An analysis of these hypotheses and the physical pattern of the processes occurring in the jet in the interelectrode gap and after the jet leaves the gap suggests that all of the above-mentioned mechanisms of jet disruption can take place and occur simultaneously. For this reason, the authors of [3÷7] used the generalized term "current instability of a shaped-charge jet."

A paper [30] reports results of experimental and numerical studies of the effect of the three possible mechanisms a) volume disruption of SCJ, b) development of magnetohydrodynamic (MHD) instability, and c) joint manifestation of MHD instability and volume disruption.

As shown by calculations, not only does an electric current accelerate the development of natural instability of a SCJ, leading to a more rapid breakup of the jet into individual fragments, but, at a sufficient strength, it can also cause the ``disc formation" phenomenon (see Fig. 34).

Calculations show that MHD instability and volume disruption are manifested at the same current-pulse parameters. Results of the calculations of cavern depths h in steel and aluminum targets in the given paper performed in [30] and experimental data are given in Tables 7 and 8, respectively. The experiments were performed by the schemes shown in Fig. 1b.

Results of the calculations performed on the assumption that MHD instability develops only in the electrode gap are given in column No. 2 of Table 7, and values of h obtained on the assumption that MHD instability develops not only in the electrode gap but also in motion of the SCJ inside the cavern are given in column No. 3 .It follows from the Tables that for a steel target (Table 7), simultaneous allowance for the two mechanisms of SCJ disruption - development of MHD instability and volume disruption - gives the best agreement between the experimental and calculated depths of SCJ penetration into the target.

For an aluminum target (Table 8), the best agreement between the experimental and calculated depths of SCJ penetration into the target is achieved on the assumption that only MHD instability is developed, provided that the current flows in the jet in its motion inside the cavern.

Table 7

Experiment		Volume destruction		MHD Inst, (Δ)		MHD Inst. (cavern)		MHD Inst.+ Volume destruct.	
		1		2		3		4	
No.	*h*, mm	*h*, mm	Δ*h*, %	*h*, mm	Δ*h*, %	*h*, mm	Δ*h*, %	*h*, mm	Δ*h*, %
98	79	82	+4	160	+103	54	-32	82	+4
101	91	132	+45	200	+120	65	-29	98	+8
103	147	184	+25	200	+36	100	-32	200	+36
102	160	200	+25	200	+25	131	-18	200	+25
116	195	200	+3	200	+3	150	-23	200	+3
contr.	205±10	-	-	-	-	-	-	-	-

Table 8

Experiment		Volume destruction		MHD Inst.+ Volume destruct.		MHD Inst. (cavern)	
No.	*h*, mm	*h*, mm	Δ*h*, %	*h*, mm	Δ*h*, %	*h*, mm	Δ*h*, %
52	257	353	+37	330	+28	257	0
53	130	353	+172	335	+158	158	+21
54	92	164	+78	144	+57	90	-2
56	93	176	+89	156	+68	91	-2
contr.	365±10	-	-	-	-	-	-

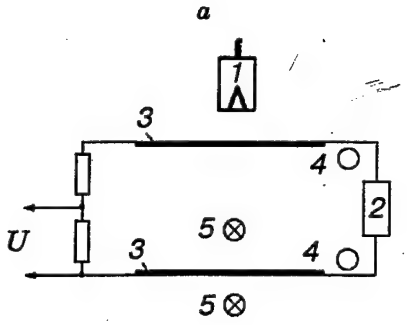

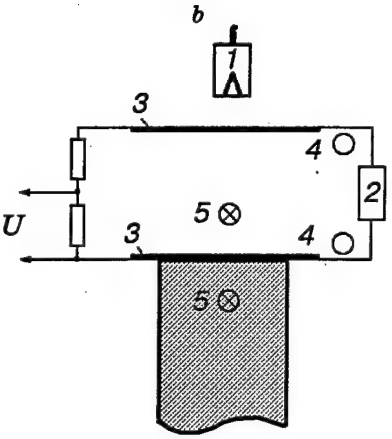

Fig. 1.

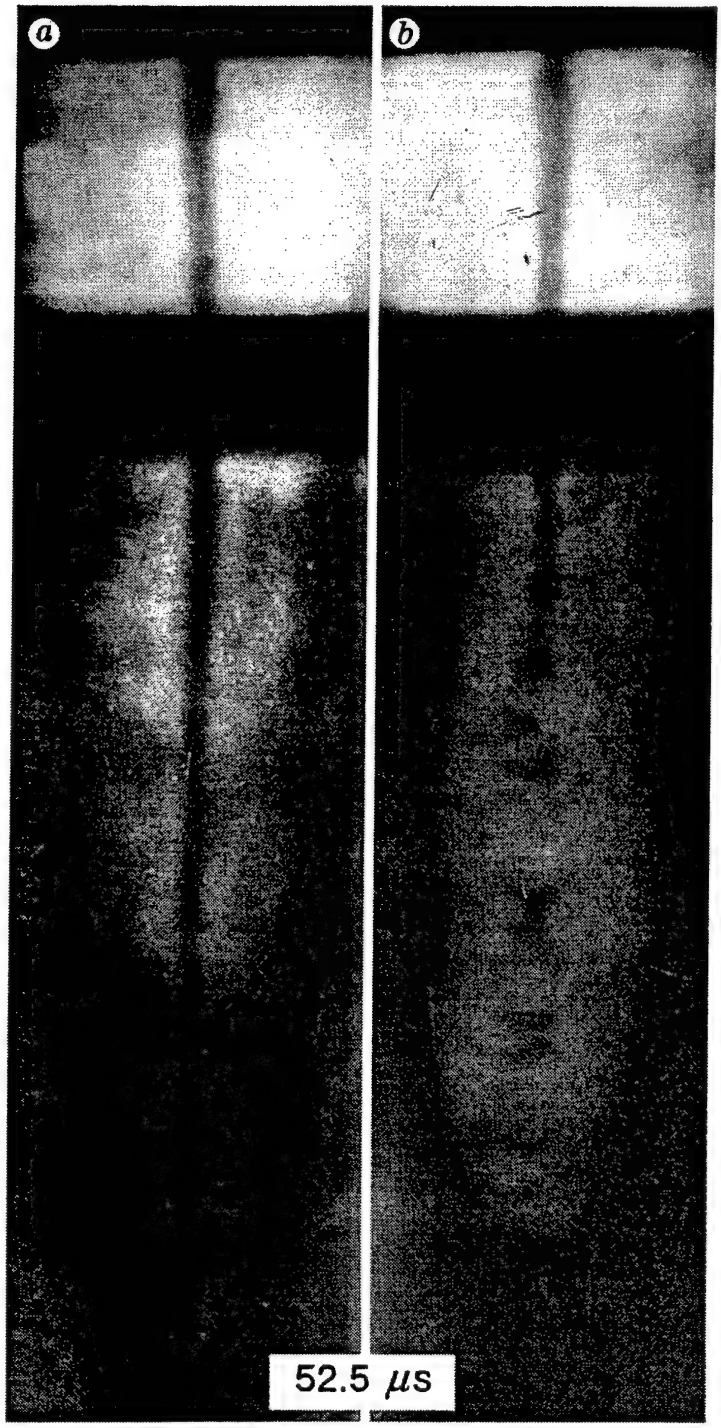

Fig. 2.

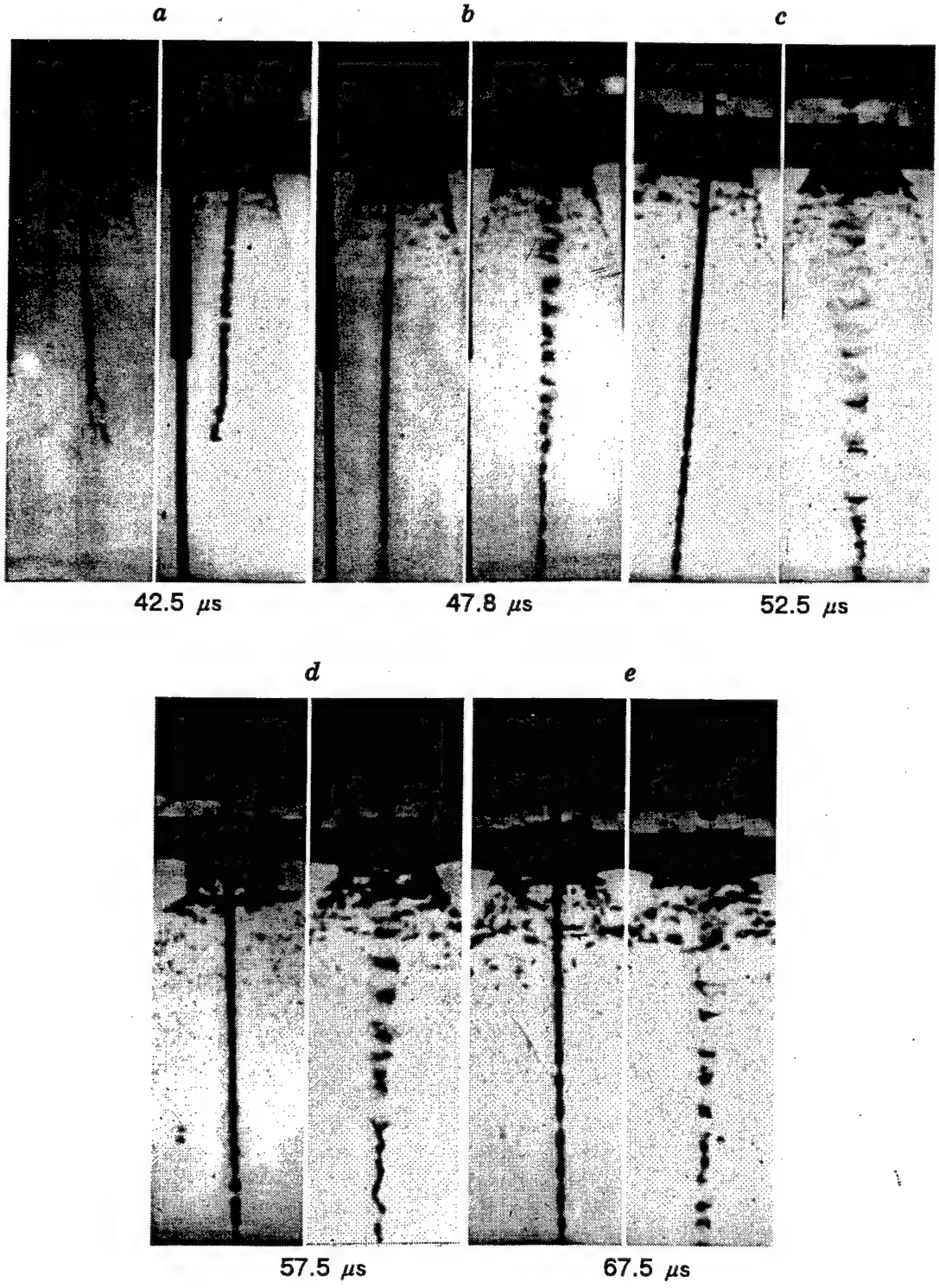

Fig. 3.

t = 52.5 μs

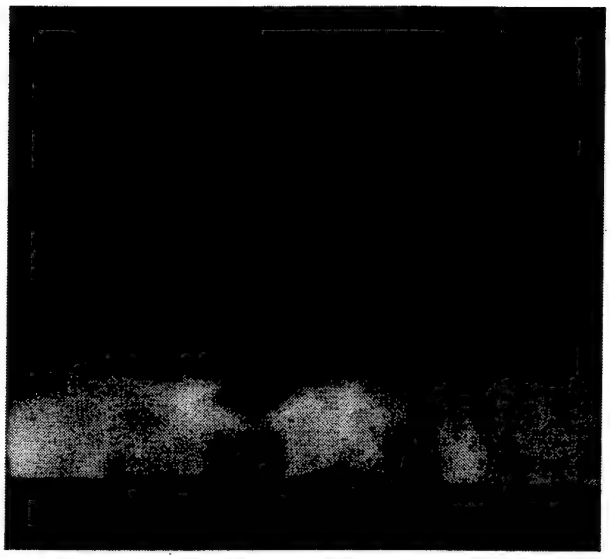

Fig. 3f.

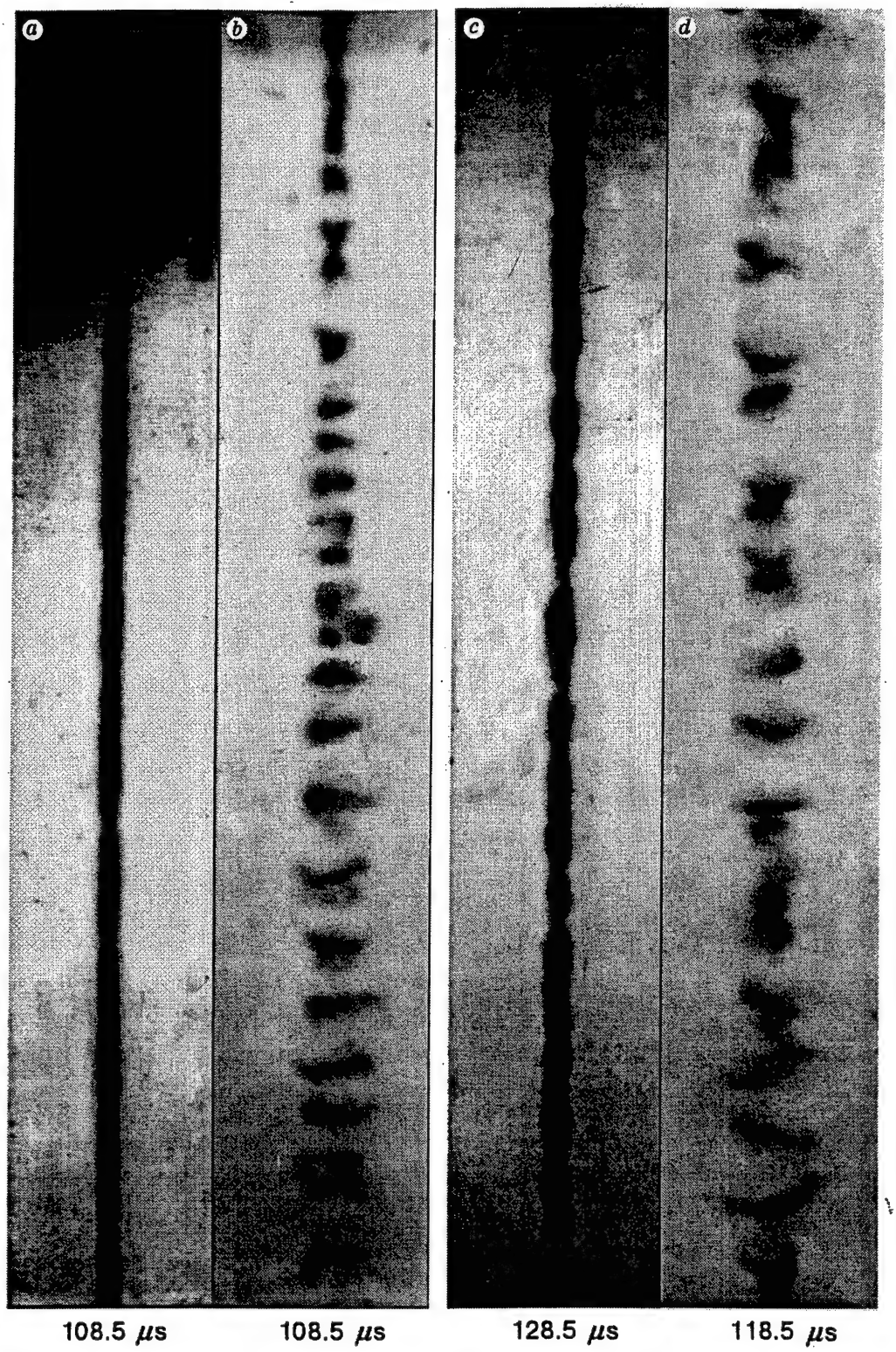

Fig. 4.

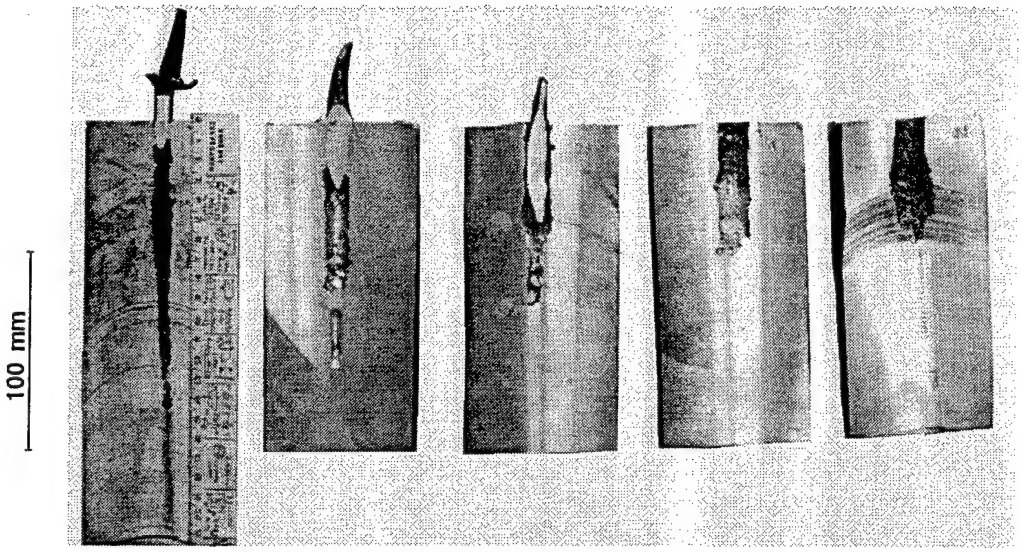

Fig. 5.

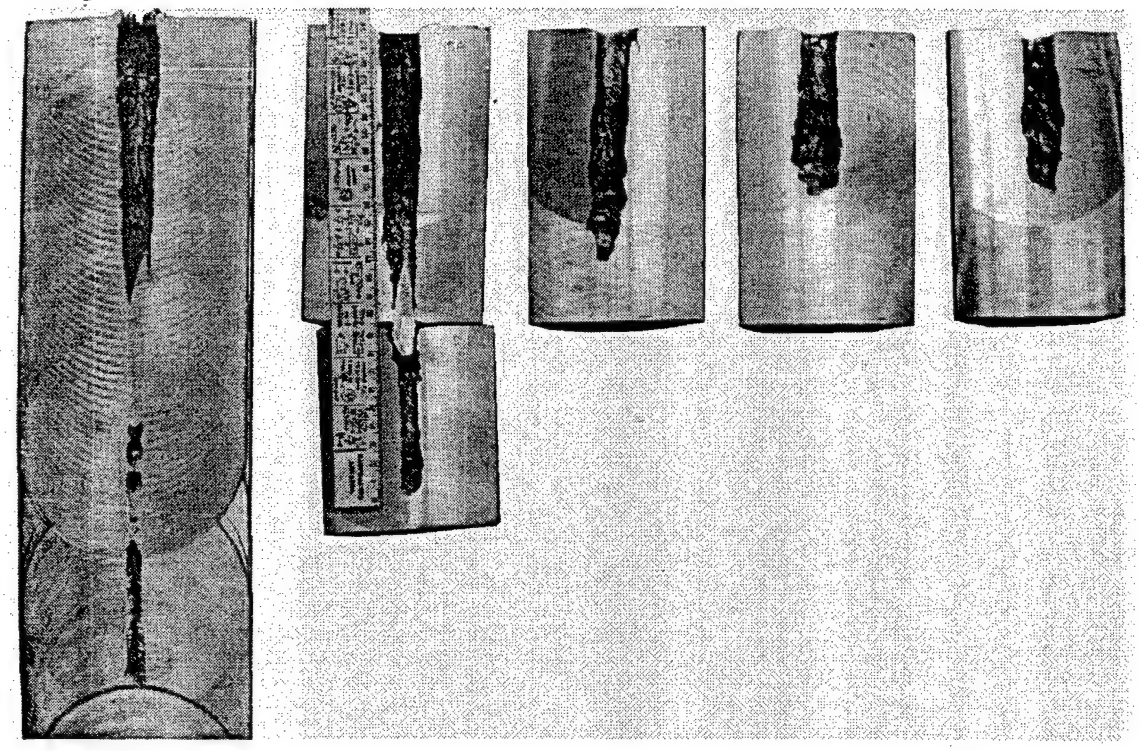

Fig. 6.

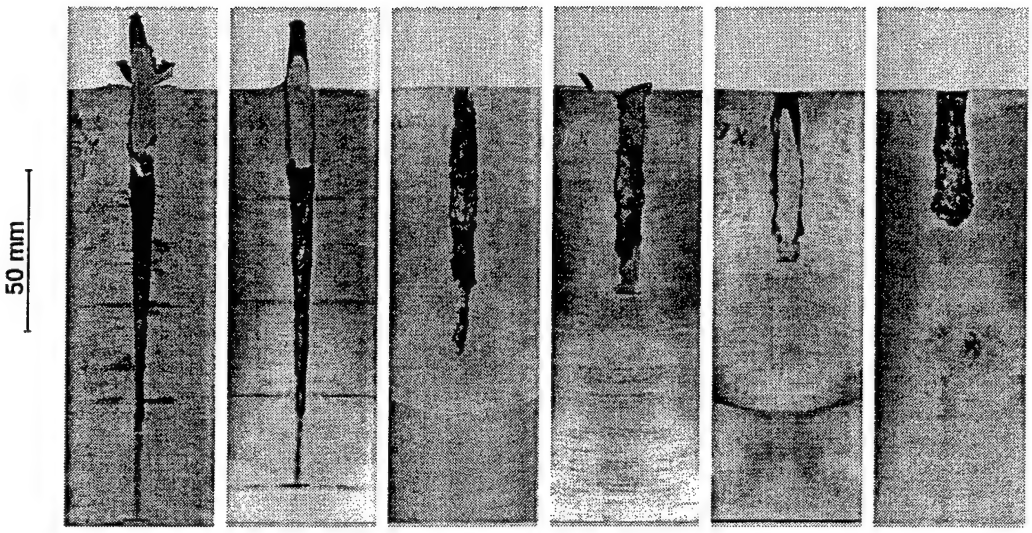

Fig. 7.

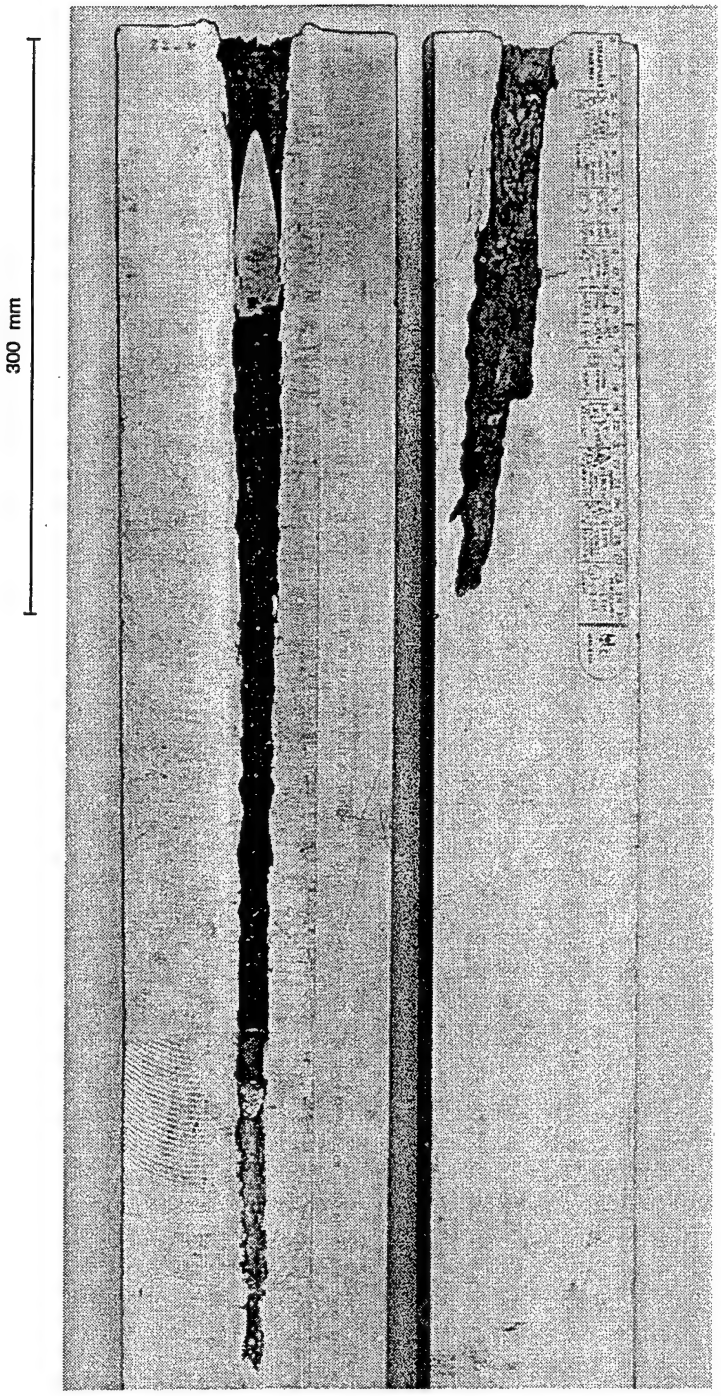

Fig. 8.

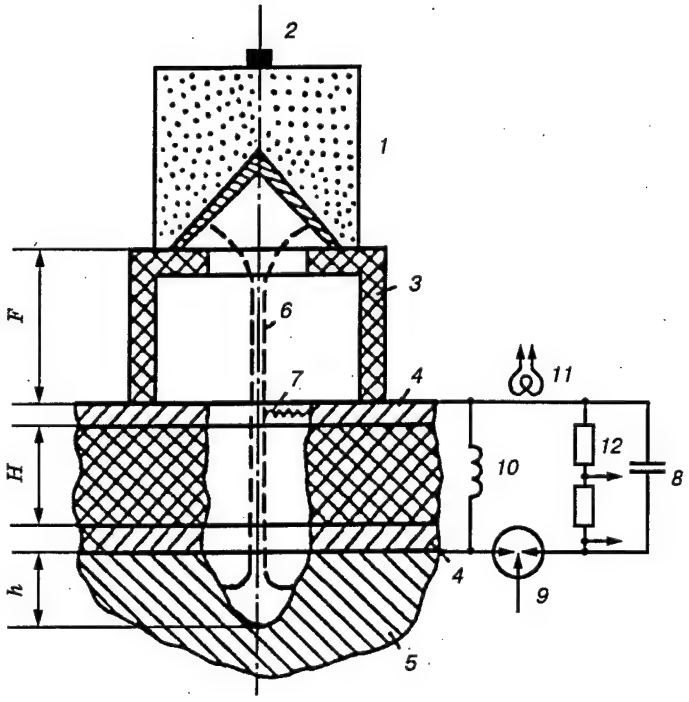

Fig. 9.

Experimental setup for studying SCJ disruption by a current pulse [8]:
1) shaped charge; 2) electric detonator; 3) support; 4) electrodes; 5) target; 6) SCJ; 7) arc discharge; 8) capacitor bank; 9) switch; 10) additional inductance; 11) inductive probe; 12) ohmic divider. For a shaped charge with a liner of diameter 45 mm, $F = 50$ mm and $H = 30$ mm, for diameter of 100 mm, $F = 115$ mm and $H = 45$ mm.

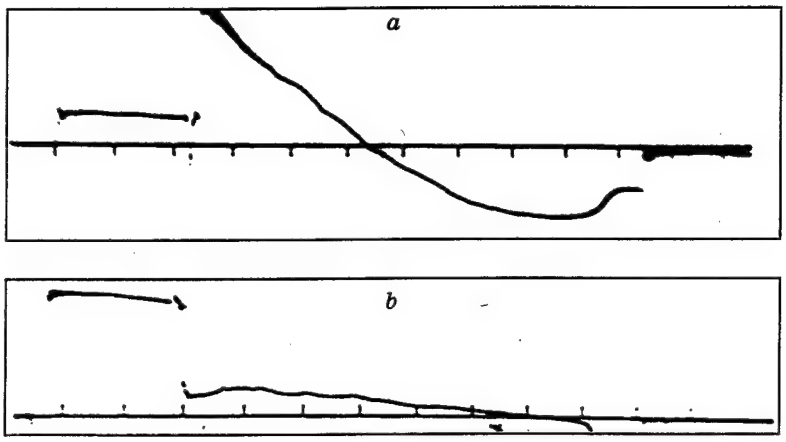

Fig. 10.

Typical oscilloscope traces of the current derivative (a) and of the voltage at the electrodes (b) [8]. The time marks are at intervals of 10 μsec.

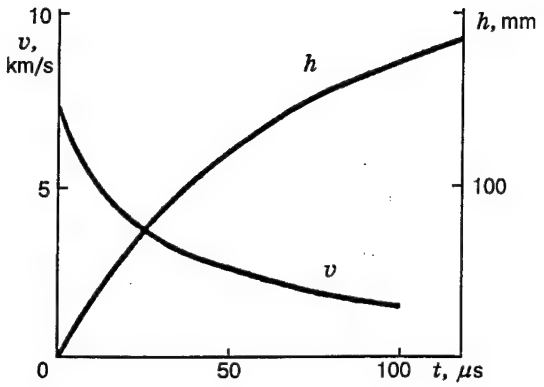

Fig. 11.

Increase in cavern depth in the target (steel3) and the jet tip velocity at this depth versus time for the SCJ of a charge with a liner of diameter 45 mm [8].

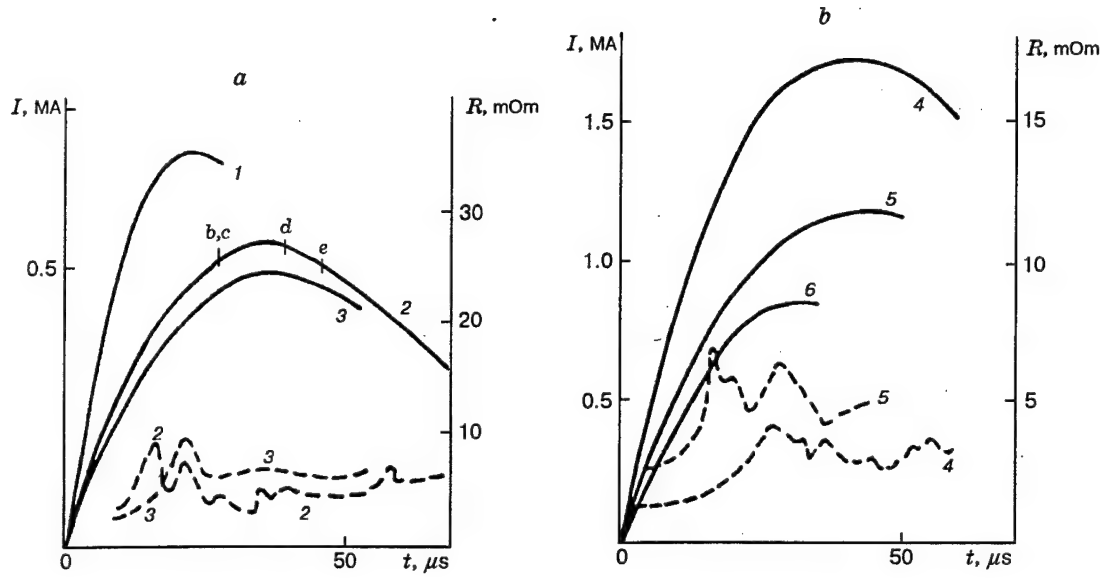

Fig. 12.

Current *I(t)* in SCJ (solid curve) and the resistance of the interelectrode circuit *R(t)* (dashed curve) [8]. The numbers correspond to the experiment numbers in Table 1.

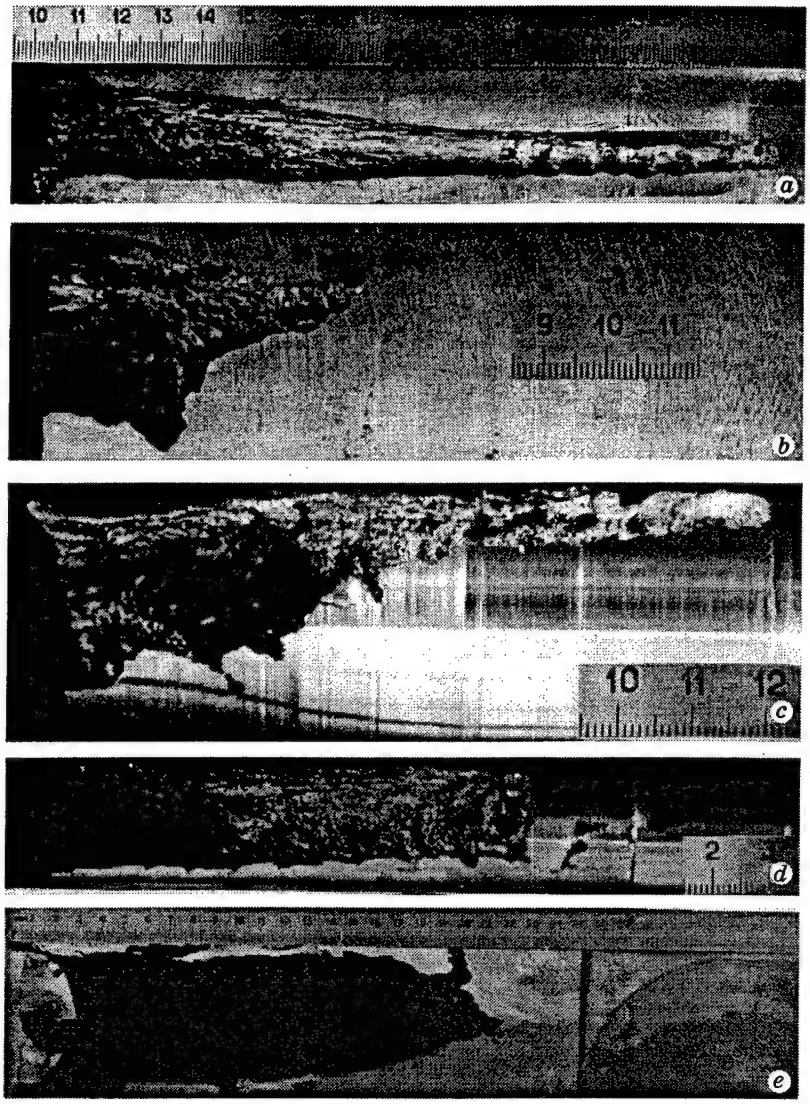

Fig. 13.

Section of caverns penetrated by SCJ in target [8]:
a) without current; b) experiment 1 (see Table 1); c) the same conditions as in experiment 1, but the capacitor bank has a smaller voltage; d) experiment 2; e) a charge with a liner of diameter 100 mm, the remaining charges, 45 mm.

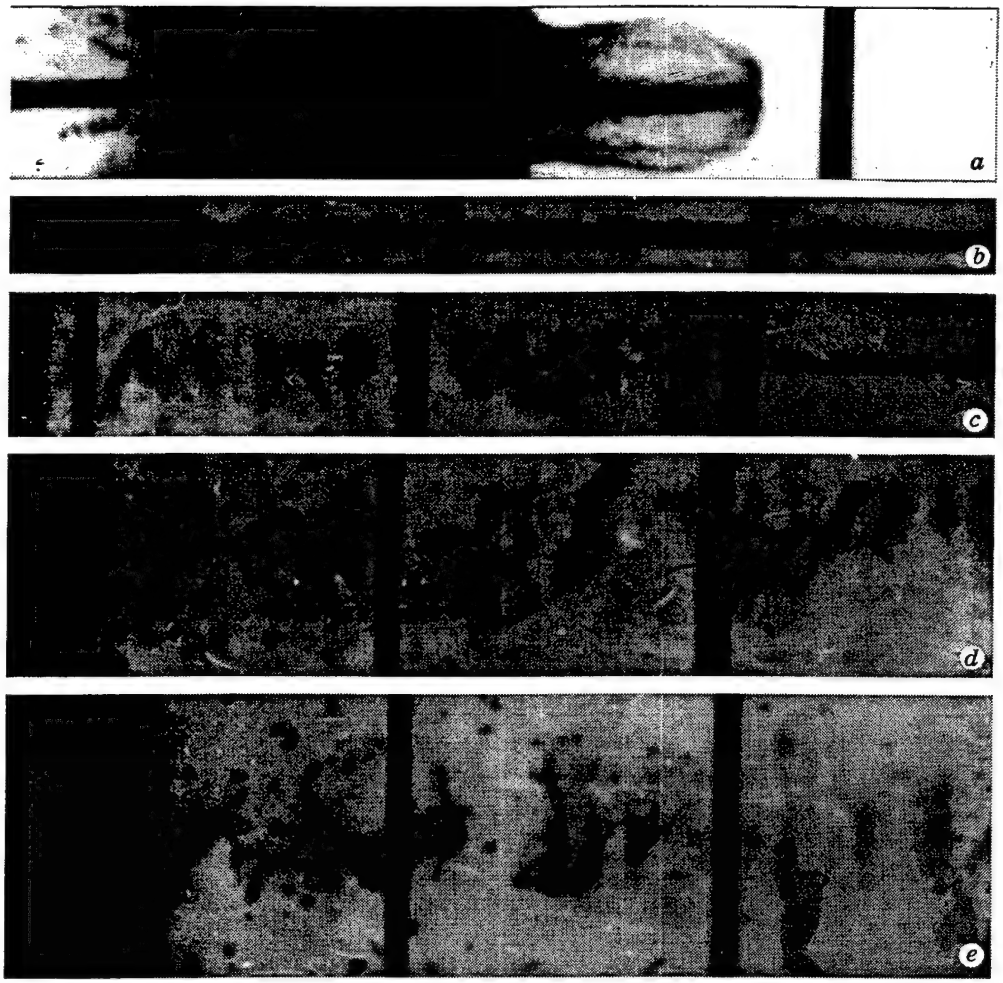

Fig. 14.

X-ray photographs of a SCJ [8]. The current in the SCJ correspond to curve 2 (Fig. 12), except for (a) and (b), where the current is diminished; a) 5 μsec; b) and c) 30 μsec, d) 37 μsec, and e) 45 μsec after passage of the SCJ the electrodes. The vertical dark stripes are cassette protection. The duration of the X-ray pulse is about 10 nsec. The diameter of shaped-charge liner is 45 mm.

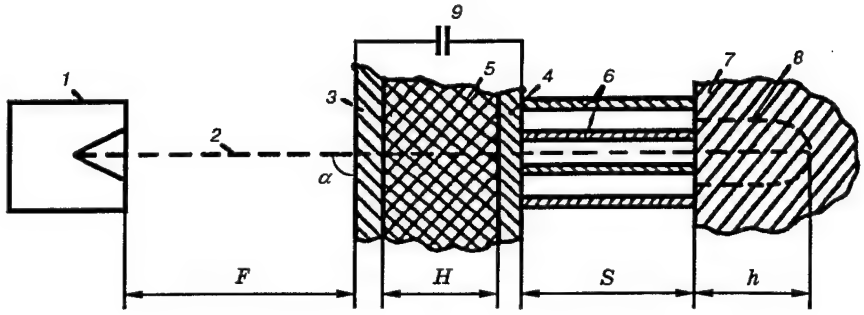

Fig. 15.

Experimental setup for studying SCJ disruption by a current pulse [9]:
1) shaped charge; 2) SCJ; 3 and 4) electrodes; 5) insulator; 6) insert (metal plates or light material); 7) metallic target; 8) cavern in the target; 9) capacitor bank; α is the angle of slope of the SCJ to the electrode plane (usually $\alpha = 90°$; in some experiments $\alpha = 30°$).

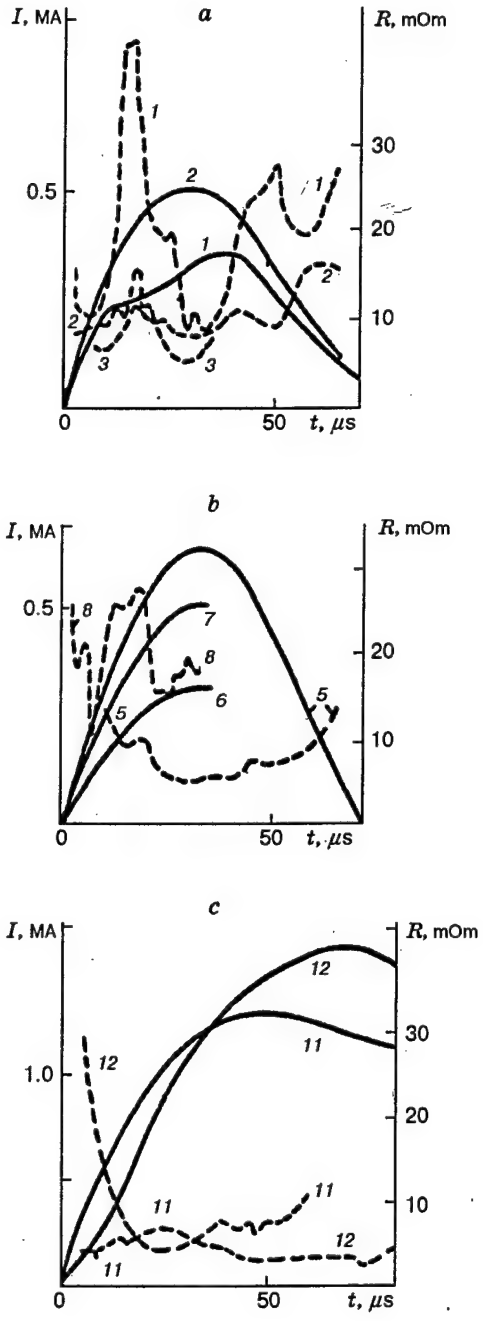

Fig.16.

Current and resistance of the interelectrode subcircuit [9]. The solid curves *I(t)* and the dashed curves, *R(t)*. The numbers correspond to the experiments numbers according to Table 2.

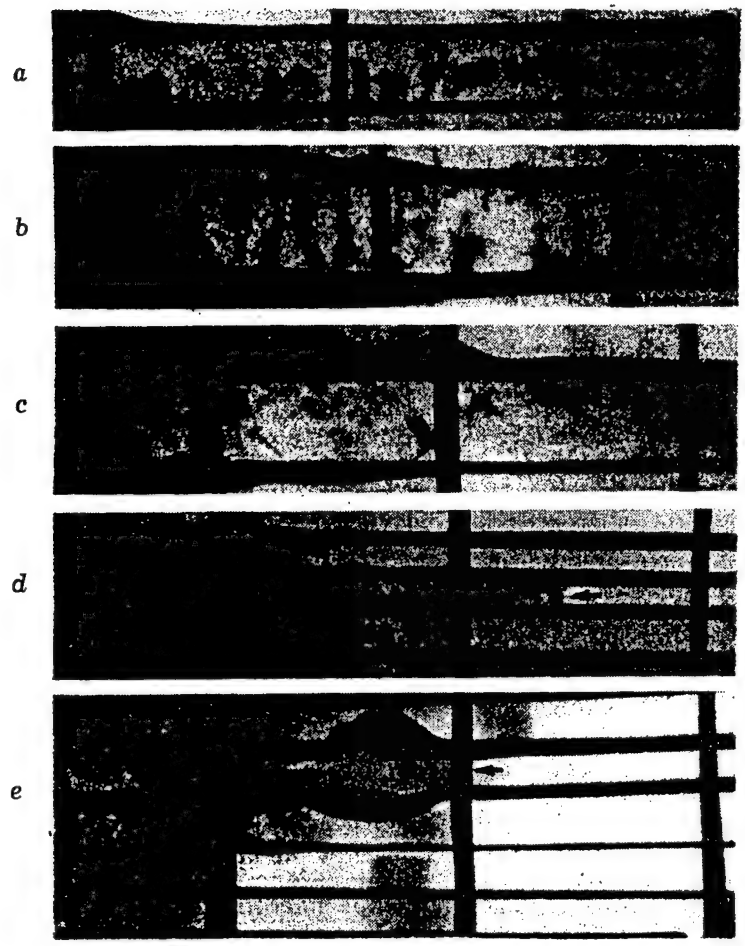

Fig. 17.

X-ray photographs of SCJ [9]. The arrows show the direction of the leading part; a) experiment 5 (see Table 2) at 25 μsec after the beginning of discharge of the capacitor bank; b) experiment 5 at 35 μsec; c) experiment 6 at 45 μsec; d) experiment 6 at 15 μsec; e) experiment 10 at 24 μsec.

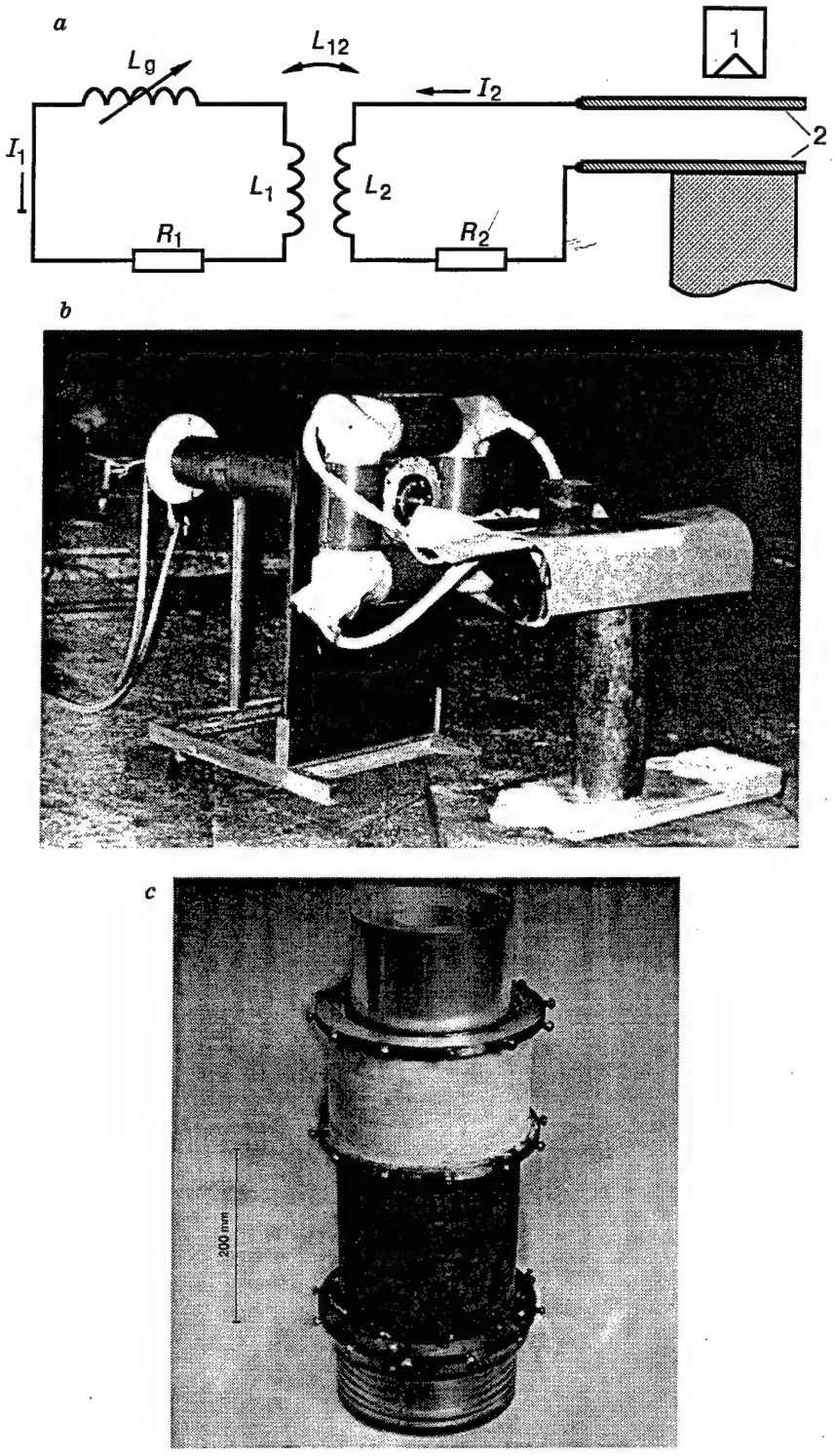

Fig. 18.

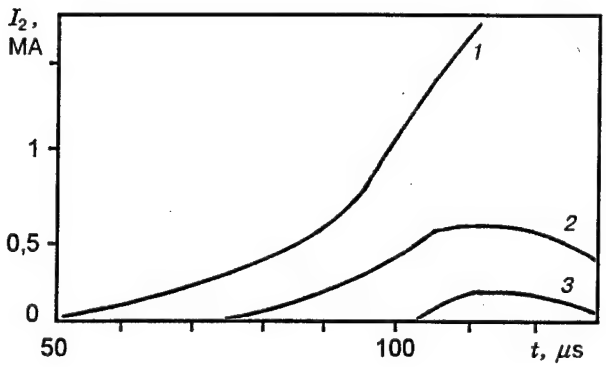

Fig. 19.

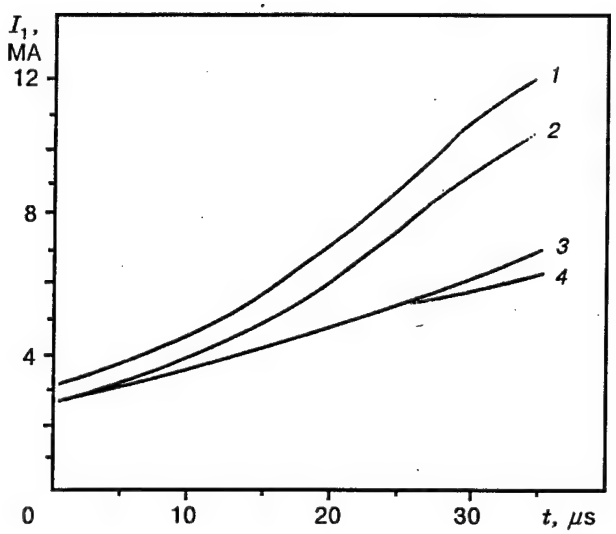

Fig. 20.

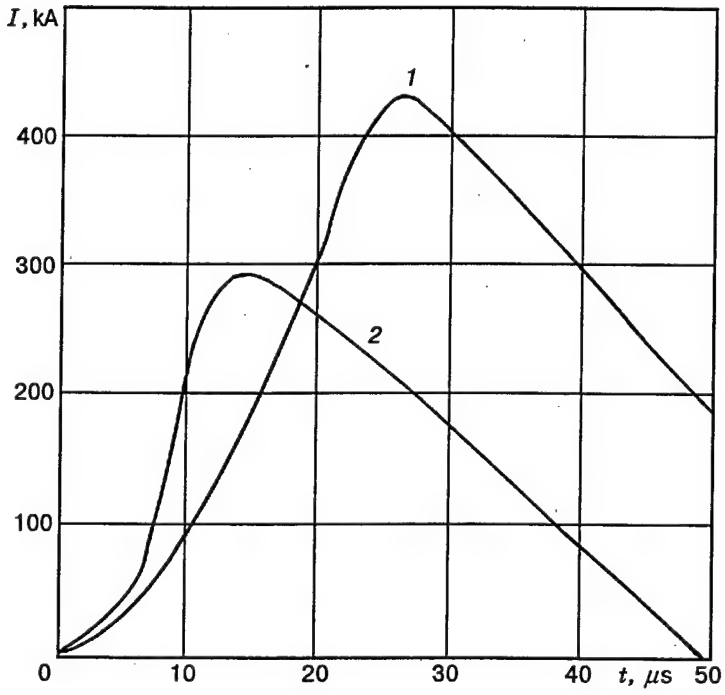

Fig. 21.

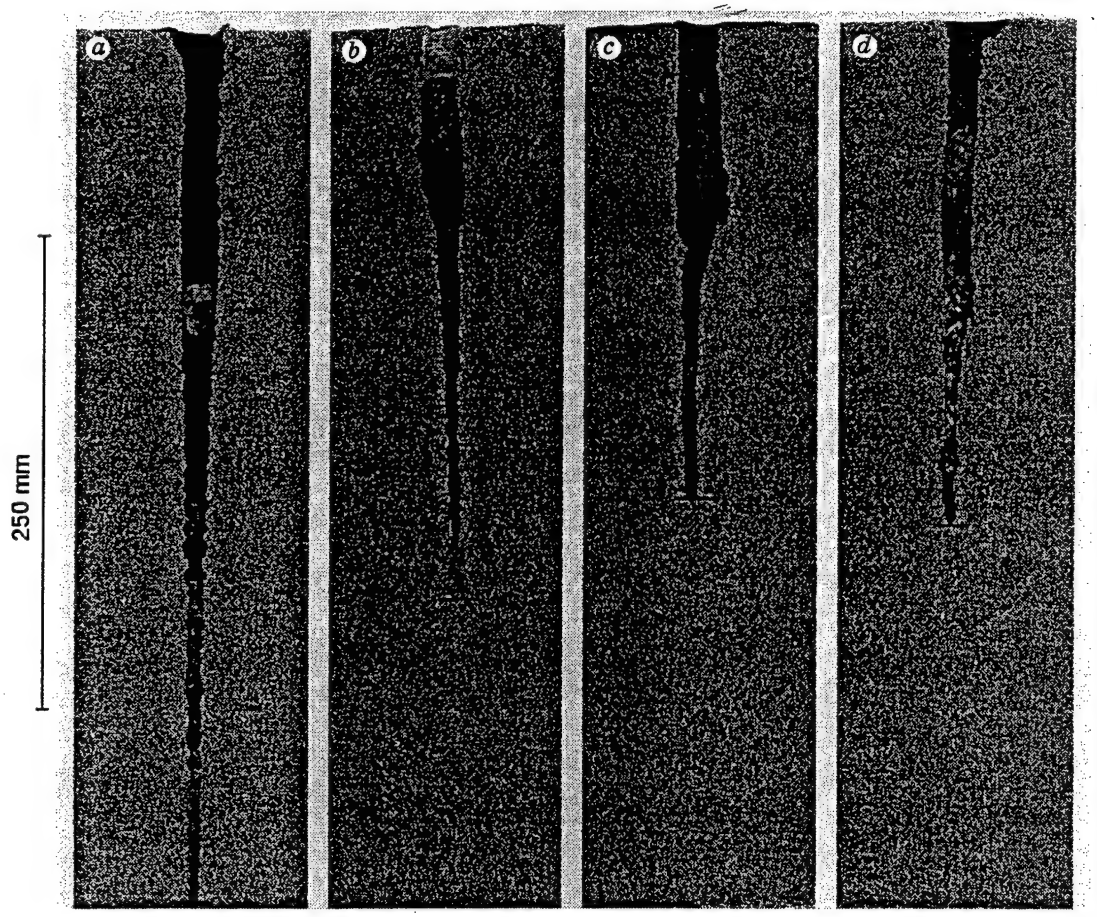

Fig. 22.

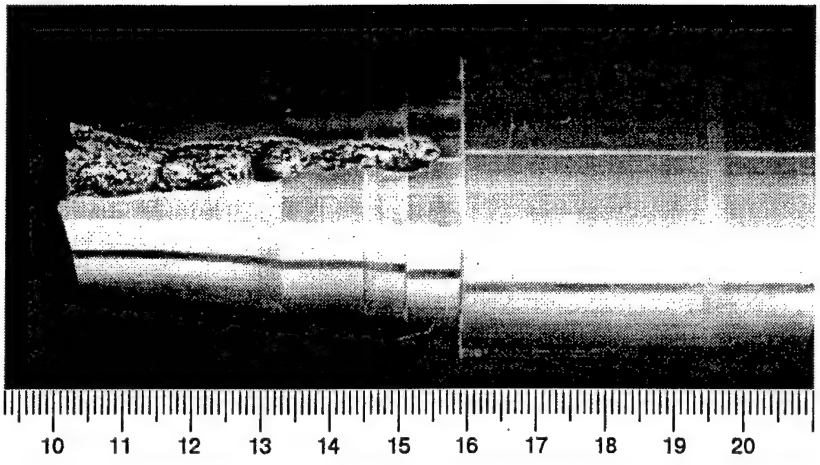

Fig . 23.

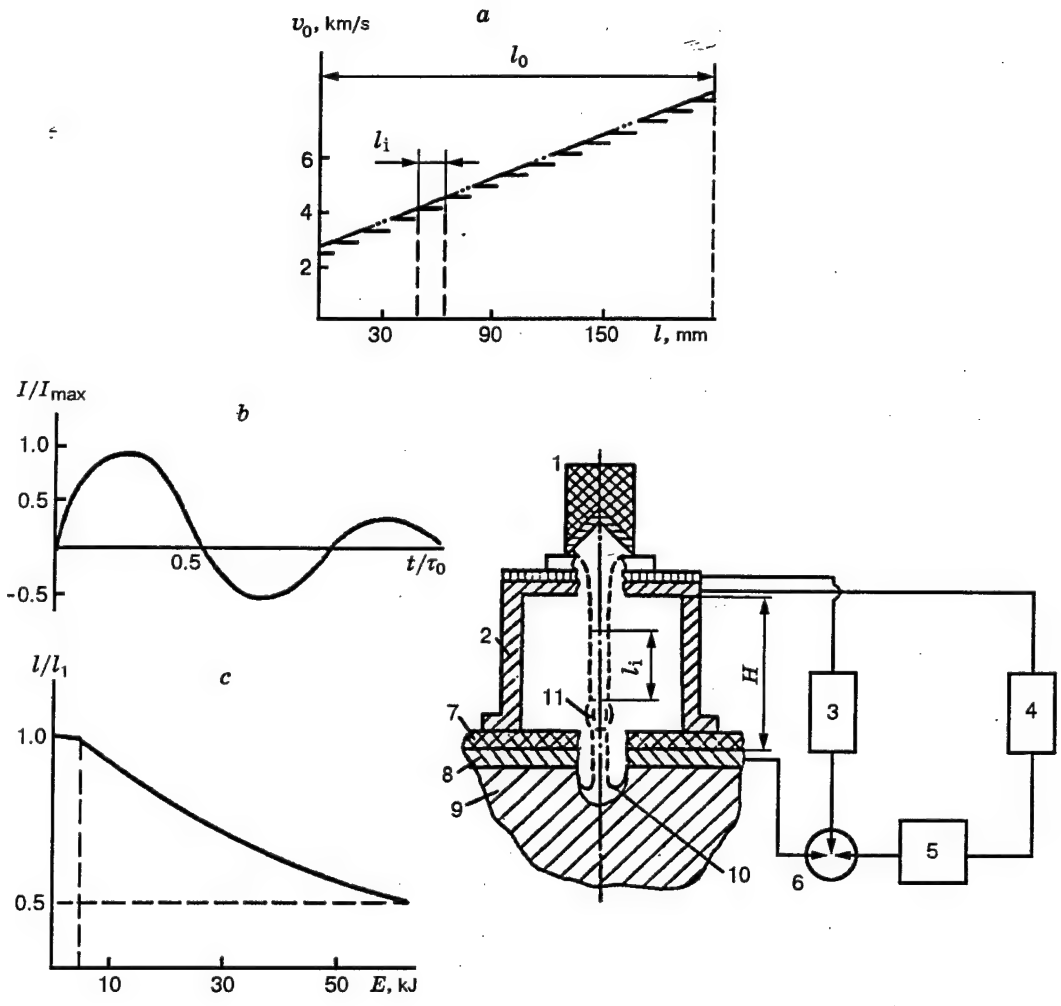

Fig. 24.

Experimental setup for studying SCJ disruption by a current pulse [17]:
1) shaped charge; 2) electrode; 3) control unit; 4) capacitor bank ($C = 4 \cdot 10^{-3}$ F, $U = 0 \div 5$ kV, $0.5CU^2$ up to 50 kJ); 5) load; 6) switch; 7) insulator (Teflon); 8) lower electrode; 9) target; 10) SCJ; 11) arc discharge. The inserts show the velocity distribution for elements of the SCJ formed by a 50-caliber charge (l_i from 10 to 18 mm) (a); the discharge current versus time (the inductance of the system is ~ 10^{-6} H and resistance is ~ $3.5 \cdot 10^{-4}$ Ohm, $\tau_0 \sim 10^{-4}$ sec (b); the depth of penetration L of copper SCJ into a copper target (c).

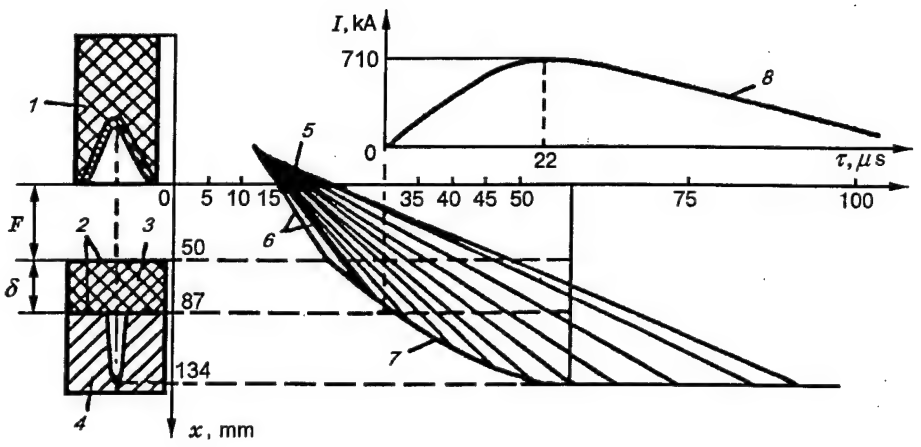

Fig. 25.

Space-time diagram of the action of an electric current on SCJ [18]:
1) shaped charge; 2) electrodes; 3) insulator; 4) target; 5) diagram of collapse of elements of the shaped-charge liner; 6) the motion trajectory of SCJ elements; 7) diagram of SCJ penetration into the target; 8) current waveform.

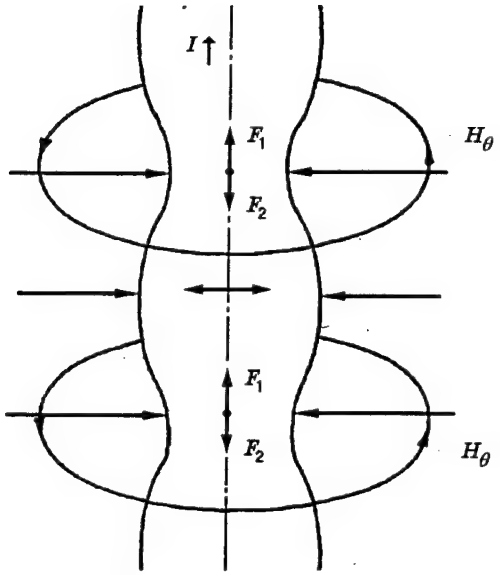

Fig. 26.

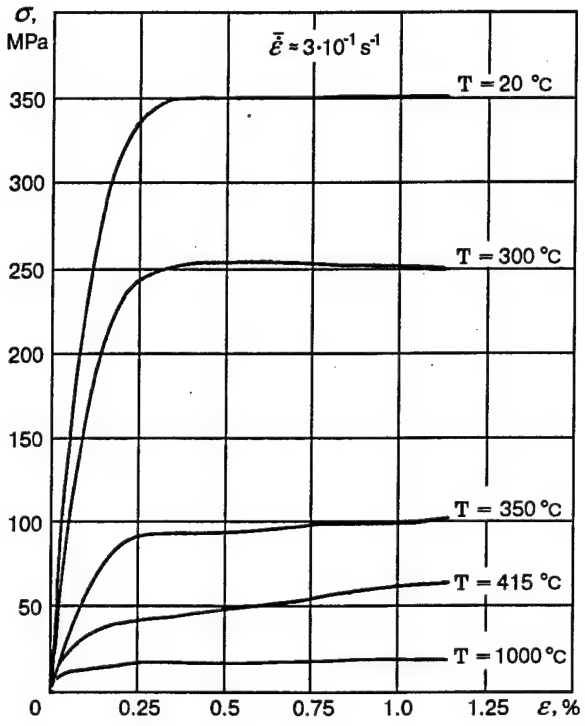
σ, MPa
$\bar{\dot{\varepsilon}} \approx 3 \cdot 10^{-1}\ s^{-1}$
T = 20 °C
T = 300 °C
T = 350 °C
T = 415 °C
T = 1000 °C
350
300
250
200
150
100
50
0
0.25
0.5
0.75
1.0
1.25
ε, %

Fig. 27.

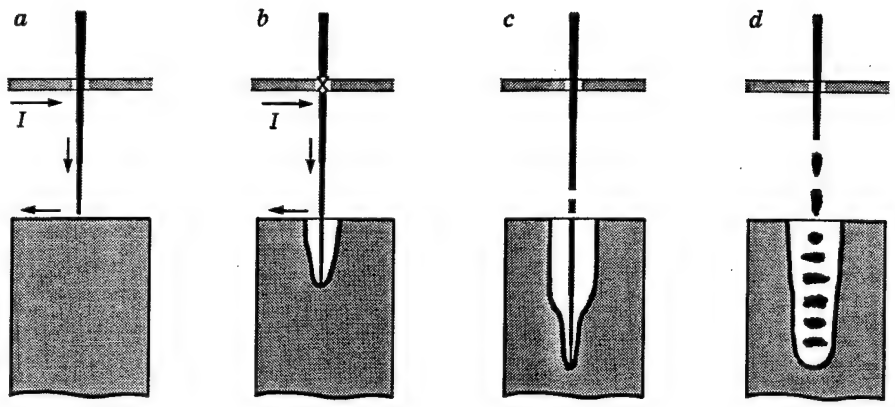

Fig. 28.

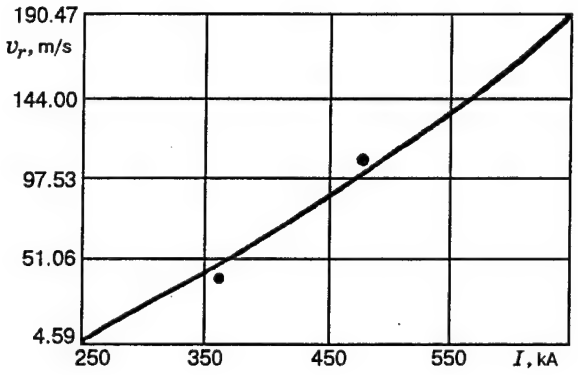

Fig. 29.

Radial scattering velocity versus the discharge current value at the moment the element emerges from the region of action [24].
—, • - analytical and numerical solutions.

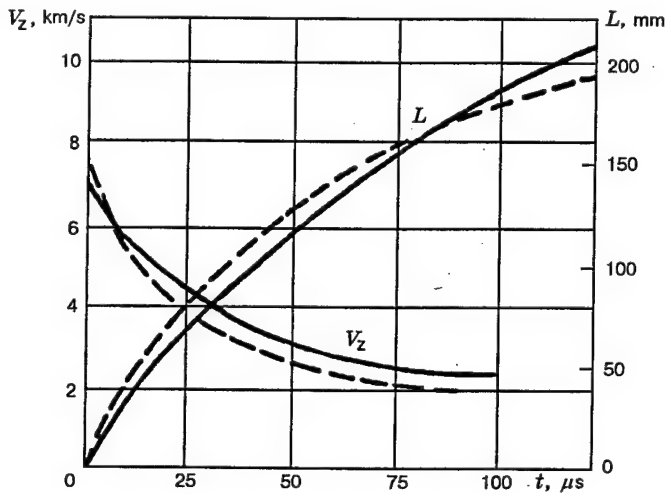

Fig. 30.

Comparison of calculated and experimental data for the penetration depth and the velocity of the penetrating element of SCJ as a function of the penetration time [24].
—- experiment; ---- calculation.

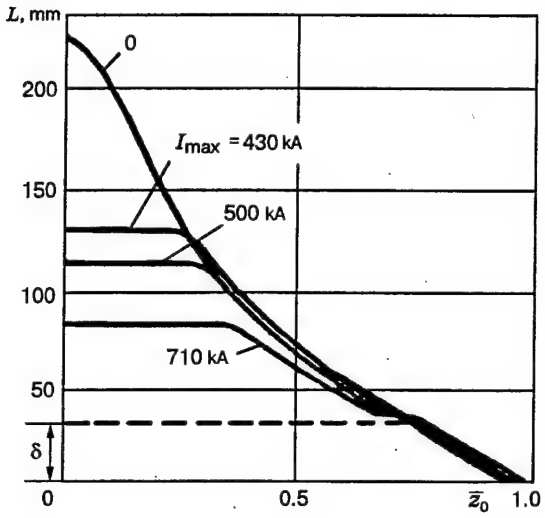

Fig. 31.

The penetration depth with serial operation of SCJ parts for different values of current [24].

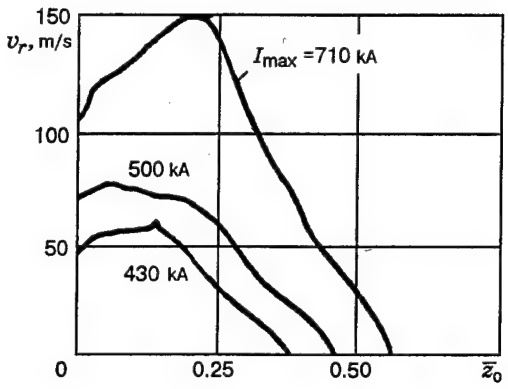

Fig. 32.

The radial velocity of the SCJ part after volume destruction for different values of current [24].

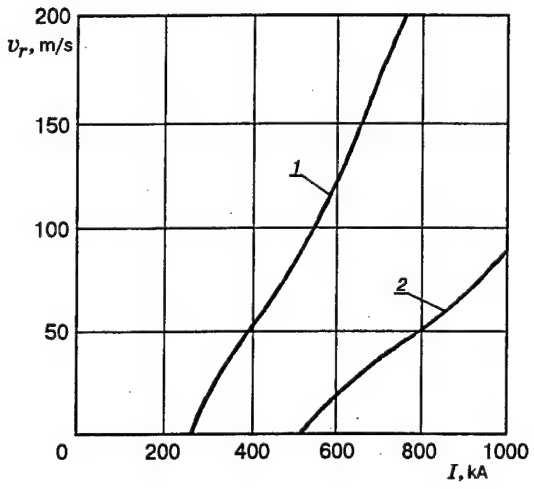

Fig. 33.

The radial velocity of scattering of the SCJ material versus current for 50-mm (1) and 100-mm (2) charges [18].

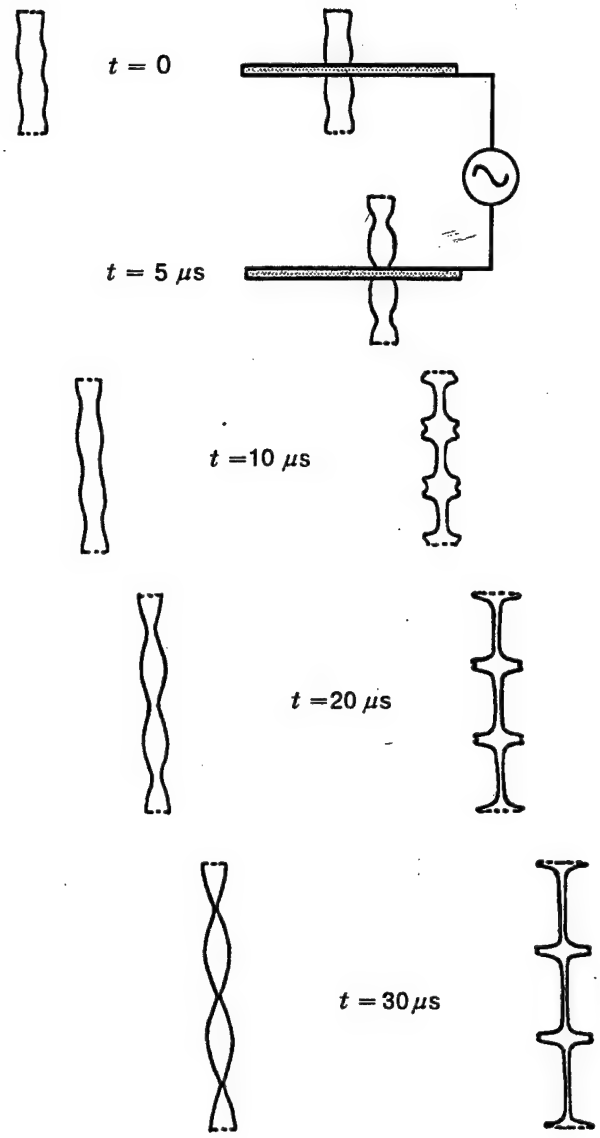

Fig. 34.

Change in the shape of the SCJ elements [18]: left - without current, right - with current.

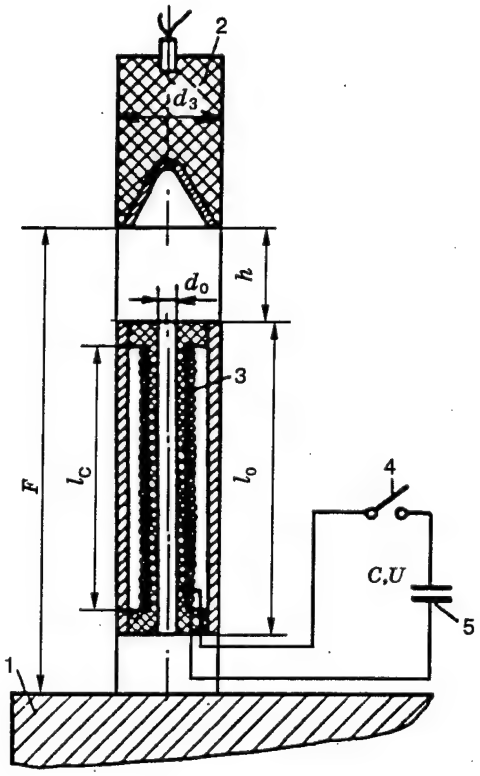

Fig. 35.

Diagram of experiment with a longitudinal magnetic field [26]:
1) target; 2) shaped charge; 3) solenoid; 4) commutator; 5) capacitor bank.

REFERENCES

1. **Yu. A. Trishin**, Personal discussion, 1957.
2. **G. A. Shvetsov et al.**, Report of LIH, 1981.
3. **G. A. Shvetsov and A. D. Matrosov**, "Current instability of shaped-charge jets," Lavrentyev Readings on Mathematics, Mechanics, and Physics: Abstracts of the 4th Intern. Conf., LIH, Siberian Branch of the Russian Academy of Sciences, Novosibirsk, 132 (1995).
4. **G. A. Shvetsov, A. D. Matrosov, and A. I. Pavlovskii**, "Current Instability of Shaped-Charge Jets," Proc. 10th Pulsed Power Conference, USA, Albuquerque, 1995.
5. **A. D. Matrosov and G. A. Shvetsov**, "Experimental study of the current instability of shaped-charge jets," Prikl. Mekh. Tekh. Fiz., 9-14 (1996).
6. **A. G. Shvetsov and A. D. Matrosov**, "Experimental study of the current instability of shaped-charges," Proc. 7th International Conference on Generation of Megagauss Magnetic Fields and Related Topics, Sarov (1996) (in press).
7. **G. A. Shvetsov and A. D. Matrosov**, "Influence of an axial electric current on the stability of shaped-charge jets," Proc. 16th International Symposium on Ballistics, San-Francisco Vol. 2, 519 - 526 (1996).
8. **A. I. Pavlovskii, L. N. Plyashkevich, A. M. Shuvalov, and A. Ya Brodskii**, "Experimental studies of destruction of a shaped charge jet by a current pulse," Zh. Tekh. Fiz., 64, No. 2, 76-82 (1994).
9. **A. I. Pavlovskii, L. N. Plyashkevich, A. M. Shuvalov, and A. Ya. Brodskii**, "Investigation of some features of the destruction of a shaped charge jet in the high current mode," Zh. Tekh. Fiz., 64, No. 5, 43-48 (1994).
10. **L. N. Plyashkevich, A. M. Shuvalov, V. V. Shutov, G. M. Spirov**, "Experiments with current destraction of jets of small-dimensions cumulative charges," Proc. Of the 8-th Itern. Conf. on Megagauss Magnetic Field Generation and Related Topics, October 18-23, Tallahassee, Florida, USA (1998) (in press).
11. **G. A. Shvetsov, Yu. L. Bashkatov, A. D. Matrosov, A. I. Pavlovskii, R. Z. Lyudaev, L. N. Plyashkevich, A. M. Shuvalov, G. M. Spirov, N. P. Shishaev, and V. V. Chivilev**, "Use of MCG in experiments on current destruction of jets," Proc. 7th Intern. Conf. on Generation of Megagauss Magnetic Fields and Related Experiments, Sarov (1996) (in press).

12. **G. A. Shvetsov, Yu. L. Bashkatov, A. D. Matrosov, A. I. Pavlovskii, R. Z. Lyudaev, L. N. Plyashkevich, A. M. Shuvalov, G. M. Spirov, N. P. Shishaev, V. V. Chivilev,** "Application on explosive MCG in experiments on current disruption of shaped-charge jets," Proc. 2-th Inter. Conf. All Electric Combat Vehicle, June 8-12, 345-350 (1997).
13. **G. A. Shvetsov and A. D. Matrosov**, "Explosive MC generator with external excitation," in: Ultrapower Magnetic Fields. Physics. Engineering. Applications [in Russian], Ed. V. M. Titov and G. A. Shvetsov, Nauka, Moscow, 263-264 (1984).
14. **A. I. Pavlovskii, R. Z. Lyudaev, L. N. Plyashkevich et al.**, "Magnetocumulative Generator with Transformer Output of Energy," in: Megaguss Physics and Technology (Ed. P. J. Turchy), N. Y.-L., Plenum Press, 611-626 (1980).
15. **A. I. Pavlovskii, R. Z. Lyudaev, L. N. Plyashkevich, and V. E. Gurin,** "Magnetocumulative generator" Inventor's Certificate No. 266100, BI, 11, 1970.
16. **L. N. Plyashkevich, I. L. Zhil'tsovs, and O. V. Rymar'**, "Modeling of a magnetocumulative generator with a transformer output of energy, Electricity, No. 7, 17-21 (1993).
17. **G. N. Yanevich, A. S. Balankin, A. A. Lyubomudrov, and I. T. Sevryukov**, "Problem of stability of a shaped-charge jet, "Zh. Tekh. Fiz., 60, No 8, 201-204 (1990).
18. **A. V. Babkin, V. A. Kruzhkov, S. V. Ladov, V. M. Marinin, S. V. Fedorov**, "The behavior of metallic shaped-charge jets under the action of a current pulse", Proc. 7th International Conference on Generation of Megaguss Magnetic Fields and Related Experiments, Sarov (1996) (in press).
19. **Physics of Explosion** [in Russian], Ed. K. P. Stanyukovich, Nauka, Moscow (1975).
20. **W. P. Walters and J. A. Zukas**, Fundamentals of Shaped Charges. New York, John Wiley and Sons (1989).
21. **Physical Quantities**, Handbook [in Russian], Ed. I. S. Grigoreva and E. Z. Melikhova, Energoatomizdat, Moscow (1991).
22. **A. V. Babkin, V. A. Kruzhkov, E. V. Lugovoi, S. V. Fedorov**, "Mathematical modeling of elongation of a shaped-charge jest with passage of an electric current through it", Oboron. Tekh., No. 9, 36-39 (1993).
23. **A. V. Babkin, M. E. Kolychev, V. A. Kruzhkov, V. M. Marinin, S. V. Fedorov**, "One possible mechanism of destruction of a shaped-charge jet under a current pulse," Lavrentyev Lectures on Mathematics, Mechanics, and Physics: Abstracts of the 4th Intern. Conf., LIH, Siberian Branch of the Russian Academy of Sciences, Novosibirsk, 119 (1995).

24. **A. V. Babkin, M. E. Kolychev, and S. V. Ladov**, "A possible mechanism of destruction of a shaped-charge jet by a current pulse," Oboron. Tekh., No. 4, 47-54 (1995).
25. **S. V. Fedorov, F. V. Babkin, and D. S. Botkin**, "Effect of a longitudinal low-frequency magnetic field on the deformation of a shaped-charge jet in free flight," Lavrentyev Readings on Mathematics, Mechanics, and Physics: Abstracts of the 4th Intern. Conf., LIH, Siberian Branch of the Russian Academy of Sciences, Novosibirsk, 158 (1995).
26. **A. V. Babkin, V. M. Marinin, and S. F. Fedorov**, "Action of a longitudinal low-frequency magnetic field on an elongating shaped-charge jet, "Oboron. Tekh., No. 9, 40-46 (1993).
27. **S. V. Fedorov, A. V. Babkin, S. V. Ladov, and V. M. Marinin,** "Features of metall shaped charge jet deformation in longitudinal low-frequency magnetic field," Proc. Of the 8-th Itern. Conf. on Megagauss Magnetic Field Generation and Related Topics, October 18-23, Tallahassee, Florida, USA (1998) (in press).
28. **S. V. Demidkov**, "Effect of an external magnetic field on the penetration depth of shaped-charge jets," Proc. 7th Intern. Conf. on Generation of Megagauss Magnetic Fields and Related Experiments, Sarov (1996) (in press).
29. **S. V. Demidkov** "On the problem of controlling the efficiency of shaped-charge jets," Prikl. Mekh. Tekh. Fiz., V.39, No. 3. 36-43 (1998).
30. **G. A. Shvetsov, A. D. Matrosov, A. V. Babkin, S. V. Ladov, and S. V. Fedorov,** "Behavoir of metallic shaped-charge jets under the action of current pulse, " Proc. Of the 8-th Itern. Conf. on Megagauss Magnetic Field Generation and Related Topics, October 18-23, Tallahassee, Florida, USA (1998) (in press).

REPORT DOCUMENTATION PAGE

Form Approved OMB No. 0704-0188

1. AGENCY USE ONLY (Leave blank)	2. REPORT DATE	3. REPORT TYPE AND DATES COVERED
	16 Nov 1998	Final Report

4. TITLE AND SUBTITLE

Current Instability and Disruption of Shaped Charge Jets

5. FUNDING NUMBERS

F61775-98-WE042

6. AUTHOR(S)

Dr Guennadi Shvetsov

7. PERFORMING ORGANIZATION NAME(S) AND ADDRESS(ES)

Lavrentyev Institute of Hydrodynamics
15 Lavrentyev Prospekt
Novosibirsk 630090
Russia

8. PERFORMING ORGANIZATION REPORT NUMBER

N/A

9. SPONSORING/MONITORING AGENCY NAME(S) AND ADDRESS(ES)

EOARD
PSC 802 BOX 14
FPO 09499-0200

10. SPONSORING/MONITORING AGENCY REPORT NUMBER

SPC 98-4019

11. SUPPLEMENTARY NOTES

12a. DISTRIBUTION/AVAILABILITY STATEMENT

Approved for public release; distribution is unlimited.

12b. DISTRIBUTION CODE

A

13. ABSTRACT (Maximum 200 words)

This report results from a contract tasking Lavrentyev Institute of Hydrodynamics as follows: The contractor will compile all previous research conducted at the Lavrentyev Institute and other Russian Institutes in the subject area in an Interim Report. Comparison of the results of experiments, analysis of data and laboratory experiments will be conducted as described in the proposal.

14. SUBJECT TERMS

EOARD, Pulsed Power, Electromagnetics

15. NUMBER OF PAGES

69

16. PRICE CODE

N/A

17. SECURITY CLASSIFICATION OF REPORT	18. SECURITY CLASSIFICATION OF THIS PAGE	19. SECURITY CLASSIFICATION OF ABSTRACT	20. LIMITATION OF ABSTRACT
UNCLASSIFIED	UNCLASSIFIED	UNCLASSIFIED	UL

NSN 7540-01-280-5500

Standard Form 298 (Rev. 2-89)
Prescribed by ANSI Std. 239-18
298-102